A review of firebrand studies on generation and transport

Rahul Wadhwani [a,b], Catherine Sullivan [c], Amila Wickramasinghe [a,b], Matthew Kyng [a,b], Nazmul Khan [a,b], Khalid Moinuddin [a,b,*]

[a] *Institute for Sustainable Industries and Liveable Cities, Victoria University, Melbourne, Victoria, 3030, Australia*
[b] *Bushfire and Natural Hazards Cooperative Research Centre (CRC), Melbourne, Victoria, 3002, Australia*
[c] *College of Engineering and Science, Victoria University, Melbourne, Victoria, 3030, Australia*

ABSTRACT

Firebrands play a vital role in the propagation of fire by starting new fires called spotfires, ahead of the fire front during wildfire progression. Firebrands are a harbinger of damage to infrastructure; their effects particularly pose a threat to people living within the wildland-urban-interface, they can hamper the suppression of wildfire and block evacuation routes for communities and emergency services. Short-range firebrands which travel along with the wind, with little or no lofting, are particularly crucial in increasing fire front propagation and damaging structures situated close to the wildland-urban interface. In the Daylesford fire of 1962 in Australia, massive short-range spotting (the process of spot fire ignition and merging of spots caused by firebrands) occurred in the eucalyptus forest and increased the rate of fire spread by roughly three times more than that computed using an operational fire model. Similarly, long-range firebrands can be transported by the fire plume and ambient wind and can ignite new fire up to 30–40 km from the source of fire as observed in the 2009 Black Saturday fire in Australia.

A large amount of experimental research has been conducted to quantify the effects of firebrands, to develop empirical models and to benchmark results for Computational Fluid Dynamic (CFD) based fire model validations. In recent years, some CFD models have been studied primarily for their validation purposes. These studies have been reviewed here. To perform useful parametric studies of firebrand transport using CFD models as well as further development of CFD models, more targeted studies need to be conducted.

1. Introduction

Wildfire (commonly known in Australia as bushfire) is a continued and increasing threat to communities worldwide. The massive destruction and loss of life associated with wildfires such as the 2009 Black Saturday fire, Australia; the 2016 Fort McMurray fire, Canada; the 2018 Carr wildfire, USA; and the 2019/20 Black Summer fire, Australia leave people traumatised and communities in ruins. Economic losses alone can adversely affect the country's GDP; the 2016 Fort McMurray fire caused $\sim$ CAD 3.58 billion insurance payout [1]. Similarly, the 2009 Black Saturday fire resulted in 173 deaths, cost the economy AUD 4.4 billion, and caused uncountable damage to the ecosystem [2].

Sources of ignition for wildfires can either be natural or anthropogenic. Miller et al. [3] observed that majority of fire ignited in grasslands and forests in Victoria, Australia during 2002–13 have natural sources.

While, Ahrens [4] observed dominance of anthropogenic sources in the ignition of bushfires, grassfires and forest fires in the United States during 2007–11. Climate change-induced effects on wildfires are profound and expected to exacerbate further [5]. Climate change increases the frequency of hotter days and prolongs the period of drought which assists the flammability of surface fuels, thus, causing more fires and extreme fires. Jolly et al. [6] have observed a pattern in an increased frequency of wildfire with the changing climate.

In extreme fires [7,8], the fire-weather coupled process accounts for the firestorm, massive firebrand spotting, intense pyrogenic wind,[1] and strong pyro-convection.[2] Firebrands, commonly known as embers are significantly prominent in the fire spread mechanism of extreme fire behaviour [8–10]. The transport of burning material like wood chips, bark, twigs, leaves, or nuts ahead of the central fire front not only increases the fire propagation rates but can also start a new fire front,

---

separated from the central fire front; this phenomenon of surface fuel ignition is called 'spotting' [11].

While spotting assists in fire propagation, spotting also causes a severe problem in controlling fires . One fundamental method of containing a fire is using a fire break which can be natural like lakes, rivers or can be human-made like roads, forest clearings or trenches to slow down or stop the fire propagation. Firebrands, however, cross these barriers to start a new fire front posing a containment challenge for firefighters. There are various recorded instances of the above situation such as the 1982 Bright Plantation fire [12] and the 1979 Caroline fire [13].

Spotting has a profound impact on the fire propagation rate due to coalescing of spotfires, and the intensity of firebrand generation by increasing the fire size. Firebrands are also one of the primary causes of inflicting damage to structures and dwellings situated in the Wildland-urban-interface (WUI) area. For example, in the 2003 Canberra fire, the suburb of Duffy suffered most of its damage due to firebrands [14]. Approximately 47% (219 houses) of houses were destroyed, and firebrands alone contributed to 65% of the damage. A similar situation was observed in the 2007 Witch & Guejito fire in Southern California where firebrands alone destroyed approximately one-quarter of the houses (20 out of 74) [15]. Firebrands mainly ignited the vegetation near the structure which subsequently ignited the structure or by direct ignition of combustible material of structure such as decks, fences, or roofing.

To predict the wildfire risks and adopt mitigating measures, fire agencies adopt various mathematical models (with various degrees of complexity and erudition) for spotting. Simpler empirical models (mostly for how far firebrands can travel once these are generated) are often based on experimental studies (both field and laboratory scales). With the availability of large computing power, new generation Computational Fluid Dynamic (CFD) based fire models are now being developed and validated against laboratory-scale experiments to enhance the prediction and prevention ability of wildfire propagation. Firebrand physics is traditionally divided into four areas: generation, transport, deposition, and secondary ignition (spotting). CFD based fire models can incorporate all four areas. To support the development and validation of CFD based fire models, more experimental studies utilising state-of-the-art equipment are needed. However, due to the complexity involving ignition by firebrands and very high computational need for its CFD modelling, it is currently not feasible to simulate ignition by firebrands at field scale with CFD models. Therefore the immediate focus can be on firebrand generation and transport. In this review, we have grouped deposition or landing pattern with transport. Before embarking upon further expensive experimental studies (especially at field scale), it is important to collate the knowledge on the generation and transport of firebrands including parameters of spotting and factors affecting the spotting propensity which will be useful to develop future parametric studies. There have been a number of studies conducted in relation to firebrands. Henceforth, we aim to review past experimental studies involving generation and transport, developed empirical models, and various CFD models & their validations. Some existing experimental studies may support improved use of available CFD fire models. Recently, Manzello et al. [16] provided a comprehensive review of firebrand studies where the main objectives were on summaring the physical characteristics of generated firebrands and their ignition capabilities mostly based on the utilisation of NIST firebrand dragon. Unfortunately, these have limited use when utilising deterministic numerical models such as CFD models. For CFD modelling, the number of firebrand generation as a function of mass loss rate or fire intensity, wind speed, species and fuel moisture content is needed. In this review, we are focusing on these aspects which can assist their utilisation in deterministic models. Similarly, other reviews such as McCarthy et al. [17] reviewed the use of radar in the study of wildfire physics including firebrands as a scatterer. A limited review on firebrand transport was provided in Węgrzyński and Lipecki [18] and in our paper it is expanded manyfold.

2. Parameters of spotting

Spotfires start when firebrands land on an ignitable ground surface, generally covered with surface fuel and litter. The firebrands are either blown with wind or lofted with the convective plume (see schematic in Fig. 1) based on various conditions such as fire intensity, local wind speed, type of vegetation, local humidity, and temperature (often fuel moisture is considered as a proxy for local humidity, and temperature).

Spotting behaviour varies in the distance and direction from the source of fire where firebrands are produced and ignited [19–21]. Byram [22] notes that the maximum spotting distance and the pattern of spotting are two crucial parameters of fire behaviours that should be quantified for accurate fire propagation. The number of firebrands generated, their transport distances, their burning characteristics, and the probability of firebrands igniting the fuel and speed of it to develop a spotfire determine the nature, and magnitude of 'firebrand attack' on a structure in a wildfire. To understand the spotting situation, it is essential to understand the landing density, ignition propensity to cause spotfire, and conditions conducive to their growth and spread. McArthur [20] proposed that concentrations of 100 ignition points per square kilometre could produce a situation similar to a firestorm.

The probability of firebrands igniting surface fuel is influenced by local weather conditions as well as characteristic variables of firebrand and fuel bed [21,23–25]. This section highlights the parameters observed in spotting behaviour before discussing the parameters which affect such differences.

2.1. Travelling distance

Spotting type can be classified based on travelling distances of firebrands. Byram [19] first classified firebrands into two categories: long-range (in the order of a few kilometres) and short-range (0.4–0.8 km) spotting based on the distance they travel. However, Cruz et al. [26] suggested classifying firebrand spotting on the basis of the distance they travel from the point of origin into three categories: (a) short-range, (b) medium-range, and (c) long-range spotting. Fig. 1 highlights the above three classifications in a schematic layout. While Gould et al. [27] in their Project Vesta experiments defined short-range spotting <150–200 m while Cruz et al. [26] defined as < 750 m, Cruz et al. [28] observed that the short-range spotting is up to 500 m in the 2009 Kilmore East fire (Black Saturday fire), and Cheney and Bary [21] observed short-range spotting occurring to around ~100–200 m ahead of the fire front in the 1962 Daylesford fire. Although short-range spotting is believed to occur in a continuous series, unlike long-range spotting which is usually discontinuous, discrete, and separate from each other. There is empirical evidence of such spotting behaviour which was observed in the 1962 Daylesford fire [20], the 1982 Bright Plantation fire [12], the 2007 Witch & Guejito fire [15], and the 2009 Kilmore East fire [28].

Wind generally transports short-range firebrands from trees with little to no lofting. It is expected that the spotting density tends to decrease with the distance from the fire front. In drier and windier conditions, the spotting densities are found to be higher as surrounding conditions make the surface litter fuels more susceptible to ignition. Short-range firebrands are expected to have flatter trajectories and have significant unburned combustible material when landing, unlike in long-range spotting.

Fig. 2 captures short-range spotting observed in the 2018 August New South Wales fires in Australia. Firebrands emanating from tree bark inside the forest canopy, are blown away by the wind and fall ahead of the tree, igniting new fires, while the surface fire is trailing those spotfires.

McArthur [20] observed the overall rate of spread is higher with the presence of short-range firebrands. McArthur reported that, in the 1962 Daylesford fire, the rate of fire spread in Stringybark eucalyptus vegetation was around 0.89 m/s, which is three times the rate of fire spread where spotting is not an effective spread mechanism. These short-range
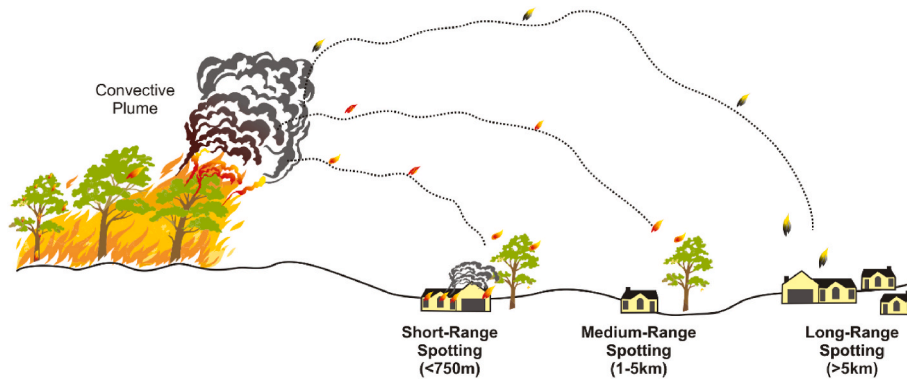
Fig. 1. A schematic layout highlighting three categories of firebrand spotting namely, short-, medium-, and long-range spotting.

Fig. 2. Short-range spotting observed inside a forest canopy in the 2018 New South Wales Fire (Photograph Credit: New South Wales RFS).

spottings coalesce with the original fire front to increase the effective rate of spread of fire. The coalescing of multiple short-range spotting results in the development of deep flaming zones, crowning and further generation of firebrands.

Cruz et al. [26] suggested a quantitative understanding of short-range spotting dynamics, namely firebrand (landing) density distribution , and how these spotfires merge with the original fire front. These are required to improve the prediction of operational fire models. The number, size, shape and firebrand density play an important role in accurate prediction for the rate of spread and hence is of high priority to assist fire managers for better estimation [29]. Kaur et al. [30] observed that when random effects of spotting and turbulence are included in an existing end-user fire model, it improved the performance of the fire model in predicting the fire perimeter qualitatively.

Medium-range spotting (1000–5000 m [26]) is the result of firebrands that are lofted briefly in the convective plume and blown away by the wind. This kind of spotting has the features of both short-range and long-range spotting. In the absence of any break in fuel or topography, isolated medium-range spotfires are run over by the original fire front. Concentrated medium-range spotting can produce firestorm[3] effects in which many coalescing fires cause strong turbulent inflow circulation resulting in a high-intensity burning [31].

Long-range spotting (>5000 m [26]) results from firebrands that are lofted in the fully developed convective plume and blown away by the wind. This kind of spotting generally starts a new fire front or damages

---

[3] A firestorm is a conflagration which attains such intensity that it creates and sustains its own wind system, commonly occurs in large wildfires.

houses which are significantly away from the fire front. Long-range spotting requires an intense fire condition that maintains a steady upward movement in the buoyant plume to transport a relatively substantial number of firebrand particles several kilometres above the ground and then intense winds to keep firebrands aloft to transport them for extended distances downwind. Long-range spotting of ~30 km has been observed several times in eucalypt forests. Long-range spotting of 30–40 km was observed in several Australian fires, such as the Kilmore region of the 2009 Black Saturday fire [28], 25 km in the 1983 Ash Wednesday fire, Victoria [32], and 29 km in the 1965 Victoria fire [20].

2.2. Direction

Byram [19] observed that in the northern hemisphere long-range spotting tends to occur on the right flank (*i.e.* towards the right direction of fire spread) of an advancing fire because the wind-velocity vector tends to advance in a clockwise direction with increasing altitude, Fig. 3. Similarly, in the southern hemisphere, long-range spotting is more likely to occur on the left flank [21]. Coriolis effect influences long-range spotting due to the firebrands' long trajectory and hence long lofted duration . However, this effect does not occur for short-range spotting which is mainly affected by the local wind condition and are at low altitude. Hence, the direction of short-range spotting occurs approximately in the direction of surface winds. Cheney and Bary [21] observed that the sector ahead of fire in which the majority (~95%) of spotfires occurred within 16° with the direction of the wind which is possibly due to fluctuations in wind direction.

2.3. Spatial pattern

Generally, two (longitudinal) patterns of spotting are observed depending on whether the fire is dominated by the shear stress of wind or convection [19]. Short-range spotting exhibits a pattern where the concentration of spotfires decreases with the increasing distance from the fire front [19]. A similar pattern was observed by Cheney and Bary [21] for fire associated with high-intensity short-range spotting. They modelled the intensity of spotting for the 1962 Daylesford fire, which burnt eucalypt forests mainly dominated by *E. obliqua* (a stringybark type vegetation) and *E. rubida* (a candle bark type vegetation), as a function of distance ahead of the central fire front. The wind mainly drives the spotting, and they observed that spotting is concentrated in the first 100 m or so, but the frequency decreases as the distance increases. However, in Project Vesta [27] short-range spotting displayed different patterns in each of their field experiments. They observed the skewed normal distribution of several spotting frequencies with distance 150 m ahead of the fire front.

The second pattern of spotting, where spotfires occur in distinct and isolated groups at varying distances ahead of the fire, is generally associated with long-range spotting behaviour [19,21]. This pattern

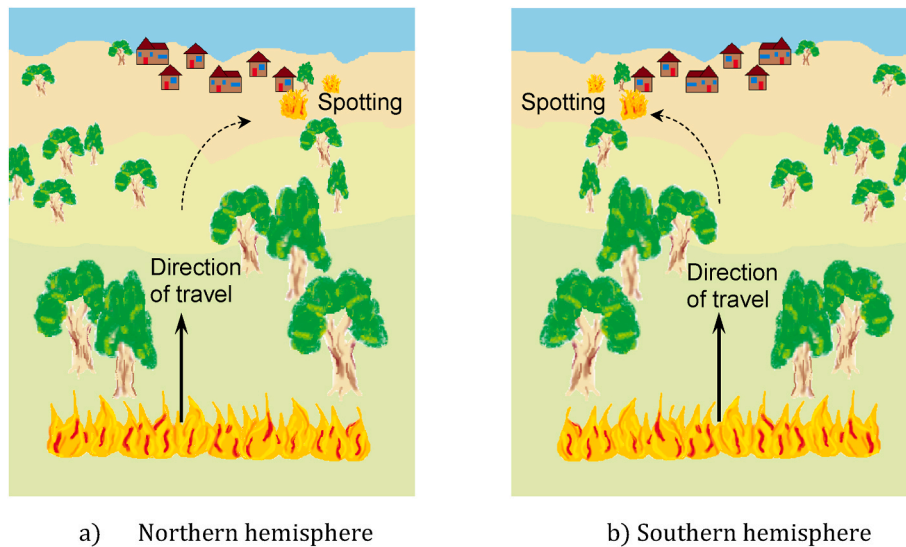a) Northern hemisphere   b) Southern hemisphere

Fig. 3. a) In the northern hemisphere long-range spotting occurs towards the right of the fire-front. b) In the southern hemisphere long-range spotting occurs to the left of the fire-front, due to the Coriolis Effect.

occurs where the fire is convection dominated which provides enough lofting to aerodynamically efficient[4] firebrands. In the 2009 Black Saturday fire, long-range spotting was observed ~30 km ahead of the central fire front [28]. Both spotting patterns can occur concurrently during one fire [21]. The lateral pattern has not been well studied in the literature.

2.4. Temporal pattern

In the 1962 Daylesford fire [20], continuous spotting at up to ~200 m occurred for at least two extended periods. Cheney and Bary [21] noted that long-range spotting frequently has a grouped and discrete distribution with each group being associated with periods of intense burning (*i.e.* the source fire) and strong convective updraughts. Reports [12,32–34] of long-range spotting indicate a discrete episodic event of spotting. Episodes of spotting could also occur when a fire hits discontinuities in fuel, and it is postulated that the subsequent decrease in fire intensity and the strength of the convection process releases large numbers of firebrands [35].

3. Factors affecting the spotting propensity

Section 2 covered the features of spotting observed in a wildfire. The spotting propensity is dependent on fire intensity, topography, firebrand material, fuel bed ignitability, and the wind field.

3.1. Fire intensity

Fire intensity is critical in the spotting behaviour, and its effect on thermal energy [36] and buoyancy [37] has been modelled. Fire intensity depends on the complex interaction of fuel with the local weather situation. Essential parameters affecting the fire intensity are fuel moisture content (FMC), local wind speed, size and amount of fuel load available, topography, and humidity which has been comprehensively discussed [19,20]. McArthur [20] modelled the effect of fire rate of spread, itself a factor affecting the fire intensity, on maximum spotting distance. Burrows [38] tabled the relationship between fire intensity,

and fire characteristics of flame length, suppression difficulty and fire effects. He observed that spotting to tens of metres could even start at low fireline intensities[5] such as 350 kW/m while long-range spotting can start at intensities higher than 2000 kW/m.

In extreme fire behaviour, where crowning occurs or in very large fires, enhanced spotting activities are observed. Spotting phenomenon is predominantly observed where significantly elevated fuels or bark fuels are available [19]. McArthur [20] found that the amount of fuel load available also significantly contributes to the spotting process. Furthermore, there is the impact of seasonal variation on the amount of surface fuel and firebrand availability [21,39,40]. Extended drought results in leaf fall, thus increasing the available surface fuel, and increasing the amount of bark that is shed for some vegetative species. The shed bark of gum species may augment the surface fuel or hanging fuels from tree trunks or branches, providing both aerial fuel and firebrand material [31].

It has been argued that concentrated short-range spotting increases the rate of fire spread and hence the fire intensity [19–21,26,41]. The concentrated short-range effect has been used to explain why an actual rate of spread differs from the predicted rate of spread [20,26,42]. The impact of coalescence of these spotfires on the fire rate of spread is one of the most challenging issues as they can dramatically increase the fire intensity thus further increasing the spotting process [26].

3.2. Wind field

Byram [22] suggested that fire intensity, thus the fire behaviour, is affected by the relationship between the rate of kinetic energy flow in the wind field (P_w) and the rate of thermal energy conversion in the convective column (P_f). When $P_f < P_w$ the fire behaviour is to be dominated mainly by shear stress of wind, and when $P_f > P_w$ the fire becomes convection dominated and increases in fire intensity [19]. The ratio of two is defined by Byram number, N_C [43,44] as described by Eqs. (1) and (2)

$$N_C = \frac{P_f}{P_w} = \frac{2gI}{\rho_a C_P T_0 (U_{10} - ROS)^3} \tag{1}$$

---

[4] The aerodynamic shapes of these firebrands are such that they experience less drag and more lift. As a result they can travel a long distance driven by convective plume and ambient wind.

[5] Fireline intensity is the measure of the rate of energy or heat release per unit length of fire front.

$$P_f = \frac{gI}{C_P T_0} P_W = \frac{1}{2} \rho_a (U_{10} - ROS)^3 \qquad (2)$$

where I is the fireline intensity, ROS is the rate of fire spread, U_{10} is the open wind speed defined normally at 10 m height, ρ_a, C_P, T_0 the density, the specific heat, and the absolute temperature of the ambient air.

The spotting distance is heavily dependent on the fire intensity and condition of the wind field. A developed convective column provides the required lofting for a firebrand to transported to a certain height after which it descends as a free-falling particle influenced by the shear stress of the wind. The fracture or collapse in the convective column due to a shear stress of wind, or ejection of firebrand from the convective column before attaining its maximum height could make firebrands drop out of the convective zone and fall early, resulting in medium-range spotting as shown in Fig. 1. Short-range spotting is mainly dominated by the shear stress of local wind with some effect of a convective column of surface fire [26] to keep firebrands afloat as observed in the 2018 NSW fire (refer to Fig. 2).

It has been proposed in a statistical model that "normal" two-dimensional convective columns lack the required uplift velocities necessary to loft firebrands large enough to ignite spotfires at a distance of more than 800 m [45,46]. The effects of turbulence are oversimplified in this approach which plays a vital role in the transport of firebrands. It was observed that firewhirls, which are three-dimensional convection columns could throw firebrands large distances and it has been proposed that this mechanism was also the cause of long-range spotting [46]. Firewhirls are often found in large fires, where they can be observed as a whirl of wind or smoke, and the intense rising heat and turbulent wind conditions can combine to form whirling eddies of air.

Spotting distance (for long-range and medium-range) is dependent on the height to which firebrands are lofted and hence the strength of the lofting process, and it appears that the fracture or collapse in this would trigger the landing of firebrands which contains sufficient energy to cause a spotfire. Byram [19] stated that the amount of spotting which occurs depends on the type of convection column and that spotting is "worse" when the shear stress of wind fractures the column. This is because those firebrands are not entirely burnt off in the convective column before they start to descend due to the collapse of this column. Cheney [35] observed that barriers to fire growth in the Southern hemisphere such as fuel reduced areas and moist southerly aspects may result in spotting behaviour that overcomes such barriers.

3.3. Firebrand material

Ignition propensity to cause a spotfire is dependent on fuel bed characteristics like FMC and humidity which has been discussed earlier in section 3.1. This section discusses mainly the properties of firebrand material.

Byram [19] stated that the fuel characteristics that make abundant and efficient firebrands are unknown. Byram suggested that charcoal, decayed wood, bark, and dry moss would be light enough to be lofted and capable of burning for several minutes thus acting as an efficient firebrand material for spotting. Firebrands are found either in the flaming or glowing state. The flaming state corresponds to the situation where the visible flame is still attached to firebrand material indicating the presence of the essential virgin pyrolyzing material. However, when firebrand material has lost its visible flame attached to the material, the firebrand is mainly composed of residual pyrolyzing material and hot char which represents the glowing state. Hence, flaming firebrands have a higher probability compared to glowing firebrands of the same size to cause a spotfire because of higher energy content. Byram [19] noted that in long-range spotting few flaming firebrands are observed while in short-range spotting (like in Fig. 2) firebrands are mostly flaming.

Albini [47] for pine plantations proposed that stemwood sections, needles, bark flakes, seed cone scales, and open seed cones have the potential to be firebrands. He proposed that a 'two-stage' firebrand, e.g.

a twig with foliage attached, might outdistance a simple wood cylinder due to the enhancement of its lofting velocity while ascending and its combustion endurance while descending.

The size of firebrands can vary substantially based on the flaming state, vegetation type, type of spotting and fire intensity. Long-range spotting requires firebrands to be lofted in the convective column with the updraught velocity which may be in the range of 110–130 km/hr [19]. Field experiments carried out in prescribed burning in pine plantations [10,48] observed firebrands ranging from few mm to few cm sizes of irregular shapes mainly made up of barks, and twigs. In the 2007 Angora fire in California, USA [49], the post-fire analysis showed that the firebrand distribution was at a point ahead of the fire front. It is estimated that most of the firebrands found to be of few mm in length and had a projected area less than 0.5 cm^2. Manzello et al. [50,51] quantified the sizes and mass distribution of firebrands produced from a pine tree. They found that most of the collected burnt firebrands are cylindrical or irregular in shape and have a higher surface area and low mass due to almost complete combustion.

Other forest vegetation species have generally lesser intense spotting behaviour as observed in the eucalypt forests in terms of spotting distance or spotfire concentration. This attribute of eucalypt forest is due to the characteristic of bark; the essential types of eucalypt vegetation have been classified according to their supposed spotting behaviour [20,21]. Bark pieces of the stringybark group and the candlebark group are suspected agents of short-range and long-range spotting [20,52]. Stringybark pieces up to 20 cm can easily be separated from the tree trunk by strong convection. However, due to higher mass they fall while coming out of the convection column as a medium-range spotting between 3 and 5 km range ahead of the fire front [31]. Tolhurst et al. [53] found that up to 7 tonne/hectare (t/ha) of this bark combusted during a mild burn in a long-unburnt forest and that this added significantly to the amount of short-range spotting. The corresponding characteristics of candlebark are its slow rate of descent, and its capacity to smoulder for long periods [21]. Hodgson [54] found that the candlebark curled into a long cylindrical shape and burned for up to 40 min and hence have significant potential to cause long-range spotting.

3.4. Size and shape

The distance up to which spotting can occur depends on the size and shape of a firebrand, the type of vegetation, fire size, and weather conditions. The size and shape of the firebrands mainly depend on the type of vegetation. For example, vegetation like *Eucalypt obliqua, Eucalypt marginata* mainly produces fibrous bark type of firebrands that are easily ignited and dislodged from the tree trunk. On the other hand, *Eucalypt globulus, Eucalypt viminalis* produces smooth decorating bark which is aerodynamically efficient and can travel longer distances.

The firebrands responsible for long-range spotting are thought to be aerodynamically efficient [23] so as to travel long distance. The long-range firebrand can be as long streamers of decorating bark that generally hangs from the upper branches in smooth-barked eucalypt species, e.g. *E. viminalis, E. globulus* [21]. The long combustion times coupled with their excellent aerodynamic properties allow these firebrands to be a viable ignition source even when transported over long distances.

3.5. Topography

A ridge or hill will tend to trigger spotting activity [20], as it attributes by increasing the fire size when the fire spreads upslope. The increase in spotting phenomena acts as a positive feedback loop in increasing the rate of spread. The effect of topography on the local wind speed and hence the fire intensity may be dramatic as observed by McCaw [55]. McCaw [55] observed spotting distances of about 200–300 m in a prescribed burn operation. In this fire, the mean fire intensities were in the range 400–600 kW/m with a short episode of high

fire intensity of 1700 kW/m due to a local topographic effect on the wind.

4. Empirical model development

Predicting the trajectory of firebrands and hence the spotting distance plays a vital role in improving the prediction of fire propagation. Koo et al. [56] have carried out a detailed discussion of various spotting models. This section discusses the major empirical spotting models developed. It is to be noted that these are mostly limited to firebrand travelling distance.

4.1. McArthur model

McArthur [20] developed a set of tables for the rate of spread, flame height, and spotting distance for given fuel quantities and conditions – referred to as the McArthur Mk.5 Forest Fire Danger Meter. These tables were later used to produce a mathematical equation, the Forest Fire Danger Index (FFDI) [57], calculated as:

$$FFDI = 2.0 * e^{\left(-0.450 + 0.97\ln(D) - 0.35RH + 0.0338T + 0.0234U_{10}\right)} \tag{3}$$

where D is Drought Factor (0–10), RH is Relative Humidity, T is Temperature (°C) and U_{10} is the open wind speed at 10 m above the ground in km/hr.

For eucalypt fuel types, containing high fibrous-bark material, the estimated spotting distance can be expressed as (Eq. (4)) [58]:

$$S = ROS(4.17 - 0.033W) - 0.36 \tag{4}$$

where S is average maximum spotting distance ahead of the source fire front (km), ROS is the rate of spread in the forward direction (km/h) calculated from FFDI ($ROS = 0.0012 \times FFDI \times W$) and W is fuel load (t/ha). Eq. (4) is derived by superimposing equations that describe the firebrand terminal velocity during flight within models of lofting mechanisms and ambient wind fields. This equation is useful mainly for long-range spotting.

4.2. Tarifa et al. Model

Tarifa et al. [59,60] plotted the trajectories for spherical, cylindrical and disk-plate firebrands in their wind tunnel apparatus to study firebrand trajectory (will be discussed in Section 5.2). In their study, they assumed that the firebrands were picked up from the ground and subsequently lofted with the convective plume column at random or due to turbulence. Tarifa et al. [59,60] ignited and combusted wood particles of different shapes to represent firebrands at their terminal velocity and constant wind speed in horizontal and vertical wind tunnels, as well as in a tapered vertical wind tunnel. Their study assumed that firebrands will always fall at their terminal velocity,[6] which can be defined as Eq. (5),

$$w = \left(\frac{2gm}{C_D A \rho_a}\right) \tag{5}$$

where, w is terminal velocity which changes with sample mass m, cross-sectional area A, drag coefficient on the particle C_D and ρ_a is the density of air. It was also identified that the drag coefficient changes little during combustion until the firebrands became exceedingly small and that the change in the size of burning firebrands in flight was the same as if they were burning in a fixed position at a constant velocity equal to their terminal velocity at that time. The loss of terminal velocity during flight for wooden spheres, cylinders, and plates is modelled as a function of the

---

[6] Terminal velocity is the highest velocity attainable by an object as it falls through a fluid (air).

parameter (Z):

$$Z = \frac{w_0 t}{D_i}\left(\frac{w_0 D_i \rho_a}{\mu_a}\right)^{-0.4}\left(\frac{\rho_a}{\rho_s}\right)^{1.3}\left(\frac{L_i}{D_i}\right)^{-0.4}\frac{l_0}{D_i}k \tag{6}$$

here w_0 is terminal velocity before its ignition, t is time including ignition time, D_i and L_i are the initial dimensions of the firebrand particle perpendicular to the wind, l_0 is firebrand particle dimension parallel to the wind, ρ_s is the density of the firebrand sample, and k is a shape factor.

In addition, they plotted trajectories using convection and wind conditions which had been recorded for actual wildfires and which varied with height. Tarifa et al. [59] also investigated the trajectories of the different shapes of firebrands such as a square wood plate, charcoal, pine cones and pine bracts of different aspect ratios and sizes.

Tarifa et al. [59] found that the critical height (Y_m) to which a firebrand could be lofted and which would result in the greatest horizontal distance (X_m) transport of firebrand is dependent on firebrand characteristics and wind conditions. The firebrand characteristics were the distance (L) of the firebrand from the edge of the convection column at the time of lofting, its function describing the change in terminal velocity with a time of flight and burning of the material. The Y_m and X_m are found to be proportional to firebrand particle density, and charcoal showed the highest amount of horizontal distance travelled. The shape of firebrands of the same nominal size exerts some influence on the transport of firebrands affecting the trajectory and distance travelled.

4.3. Albini model

Albini [47] used data collected by Muraszew et al. [61]to develop an equation for change in the product of the thickness and density of limb-wood sections burnt at constant wind velocities. Muraszew et al. studied the rate of mass loss of burning wooden dowel segments at several wind speeds to characterize the behaviour of large burning firebrands shortly after being released from a fire. This research produced a series of correlations of mass-loss rates with a dimensionless value that describes the geometry of the dowel. Using these correlations, Albini gives an equation relating the terminal velocity of these particles with time (w_t),

$$w_t = w_0\left(1 - \frac{K\pi g t}{4C_D w_0}\right) \tag{7}$$

where $K = 0.0064$ from the experiment.

Albini [47] integrated Eq. (7) for the combustion time and derived the value for the total vertical movement of air relative to the sample (Δz) as;

$$\Delta z = \frac{1}{2}w_0\left(\frac{4C_D w_0}{K\pi g}\right) = \frac{(\rho_s D)_0}{K\rho_a} \tag{8}$$

where, w_0 is initial terminal velocity, $K = 0.0064$, $(\rho_s D)_0$ is the initial product of particle density and diameter, and ρ_a is the density of air. For a lofting process of a given strength, there will be a sample of initial density and diameter that will burn out just as it reaches the ground. The optimum sample will result in the greatest potential spotting distance for the given conditions. Albini [47] modelled the maximum height $z_{(0)}$ to which samples of burning optimum size limb-wood would be lofted by one or several torching trees, or by a pile of burning timber debris [62] or by a line fire [63]. Chase [64] presented them as follows.

For a torching tree,

$$z_{(0)} = a(d_F)^b(h_F) + h / 2 \tag{9}$$

where h_F and d_F are the adjusted steady flame height (m) and adjusted steady flame duration (dimensionless), h is the height of burning trees and constants a, and b vary with the flame parameter and vegetation

type.

Further, h_F and d_F are computed as follows,

$$h_F = a_1 d_2^{b_1} n^{c_1} \tag{9a}$$

$$d_F = a_2 d_2^{b_2} n^{c_2} \tag{9b}$$

where, a_1, b_1, c_1, a_2, b_2, and c_2 are vegetation specific constants, d_2 is the diameter of a torching tree at breast height, and n is the number of trees burning simultaneously to form a single merged buoyant flame structure. For a burning pile,

$$z_{(0)} = 12.2 H_F \tag{10}$$

where H_F is the constant flame height (m).

For wind-driven surface fire or line fire

$$z_{(0)} = 0.173\sqrt{E} \tag{11}$$

where E is thermal energy strength (kJ/m).

Albini [36] assumed that thermal energy is the product of fireline intensity I_B (kW/m) and wind speed U_{10} (m/s) measured at 10 m height and is given as,

$$E = I_B\left(A_1 U_{10}^{B_1}\right) \tag{12}$$

where A_1 and B_1 are constants that change with the fuel type.

For torching tree and burning pile scenarios, firebrands are assumed to be lofted vertically, and the spotting distance is determined by this initial firebrand height ($z_{(0)}$) and the ambient wind field [47]. Chase [64] presented Albini's model in numerical form for power-law ambient wind profile,

$$S_f = 1.3 \times 10^{-3} U_6 h_*^{0.5}\left[0.362 + \left(\frac{z_{(0)}}{h_*}\right)^{0.5}\frac{1}{2}\ln\left(\frac{z_{(0)}}{h_*}\right)\right] \tag{13}$$

where S_f is the maximum spotting distance on flat terrain (km), U_6 is the mean wind speed at 6 m above the vegetation (km/h), $z_{(0)}$ is the height to which firebrands are lofted (m) and h_* is the higher value of h_1 and h_2. These latter parameters represent mean vegetation cover height (m) downwind of the source of fire, and the minimum representative height used to describe the wind profile, respectively.

For wind-driven surface fire, in Eq. (13) downwind drift of firebrand during the lofting process is also added to maximum spotting distance for the firebrands and is represented by Eq. (14)

$$S_f = 1.3 \times 10^{-3} U_6 h_*^{0.5}\left[0.362 + \left(\frac{z_{(0)}}{h_*}\right)^{0.5}\frac{1}{2}\ln\left(\frac{z_{(0)}}{h_*}\right)\right] + 5.03 \times 10^{-4} U_6 z_{(0)}^{0.643} \tag{14}$$

Chase [64] stated that these equations (Eq. (13 -14)) were unsuitable for predicting short-range spotting or very long-range spotting. Chase had personal communication with W.R. Catchpole[7] that the above equations could underpredict spotting distance in eucalypt forest which is known to produce aerodynamically efficient bark firebrands.

4.4. Ellis/Raupach model

Ellis [23] developed a two-dimensional (2D) spotting model using the wind tunnel constructed by the Commonwealth Scientific and Industrial Research Organisation (CSIRO), Australia. In his study, he combined the aerodynamic and combustion behaviours of a firebrand to estimate the spotting distance of firebrands in two different combustion patterns which affects the mass of the particle and hence the spotting pattern. This applies a correlation of the loss of terminal velocity of messmate stringybark samples on a simple wildfire plume model [37].

---

[7] Researcher at University of New South Wales, Australia.

Ellis' model [23] requires information about the above-canopy wind speed, updraft velocity, and horizontal component of velocity in the convection plume. Additionally, the initial height of the firebrand above the ground, and the initial distance between the firebrand and downwind boundary of the convection plume.

The Ellis' model [23] suggests that firebrands may land in a flaming state, a glowing state, or a reflaming state or with a certain remaining mass. The maximum distance (X_m) which is a sum of horizontal distances the firebrand is transported when inside and outside of the plume, and is computed as,

$$X_m = \left(t_{hmax} \times U_{xp}\right) + \left[(t_b - t_{hmax}) \times U_x\right] \tag{15}$$

where t_{hmax} is the time (s) from commencement of flight at which firebrand achieved Y_m, U_{xp} the horizontal component of wind velocity inside the wildfire convective plume (m/s), t_b is the burnout time in flight, after ignition, at which combustion ceases (s), U_x is the horizontal component of ambient wind speed (m/s).

Finally,

$$Y_m = \int_0^{t_{hmax}} \left(U_{yp} - w_t\right)dt + h_0 \tag{16}$$

where Y_m is the maximum height (m) to which firebrands are lofted and still be combusting till it reaches the ground, U_{yp} the vertical component of wind velocity inside the wildfire convective plume (m/s), h_0 is the initial height of firebrand above the ground (m), w_t terminal velocity of firebrand at time t second during flight and is a function of time (m/s).

Ellis [23] carried out an analysis of his spotting model, McArthur's spotting model (Section 4.1) and Albini's spotting model (Section 4.3) on the 1962 Daylesford fire. The recorded observation for maximum spotting distance in the fire was between 3600 and 4000 m. Ellis's model predicted spotting distance in the range of 2000–4800 m, McArthur's model predicted spotting more than 6500 m, and Albini's model predicted spotting to be ~1900 m. His conclusion suggests that McArthur's model overpredict the maximum spotting distance while Albini's model underpredicts it by roughly 50%. While the Ellis model makes a reasonably good prediction, it requires further verification and validation in different situations. Project Vesta [27] further tested the Ellis model in their field experiments. The quantification of firebrand spotting is one of the hardest challenges faced by Project Vesta team [27]; however, they were able to observe a spotting trend. Ellis' model tends to overpredict in most of the cases and only one case was an accurate estimate and one other was close, where it was an underprediction.

4.5. Woycheese et al. Model

Woycheese et al. [65] first published their work on firebrands lofting above large fires in the context of a structural fire. While previous studies of Tarifa et al. [59,60] and Lee et al. [66] assumed constant vertical velocity for firebrand's lofting above the fire source, Woycheese et al. [65] modelled it using an axisymmetric pool fire representing a burning house with a Baum and McCaffrey empirical plume model [67], which is more accurate. The acceleration of particles with time-dependent particle mass and velocity is expressed as Eq (17).

$$\frac{dV}{dt} = \frac{1}{2}\left(\frac{\rho_a A C_D}{m}\right)|V_r|V_r - \left(\frac{V}{m}\right)\frac{dm}{dt} - g \tag{17}$$

where, V_r is the relative velocity of the plume to the particle, V is the particle velocity, m is the mass of the sphere and A is the cross-sectional area of a sphere.

From Eqn (17) and applying boundary conditions, the maximum loftable height (Y_m) of a spherical particle was determined as
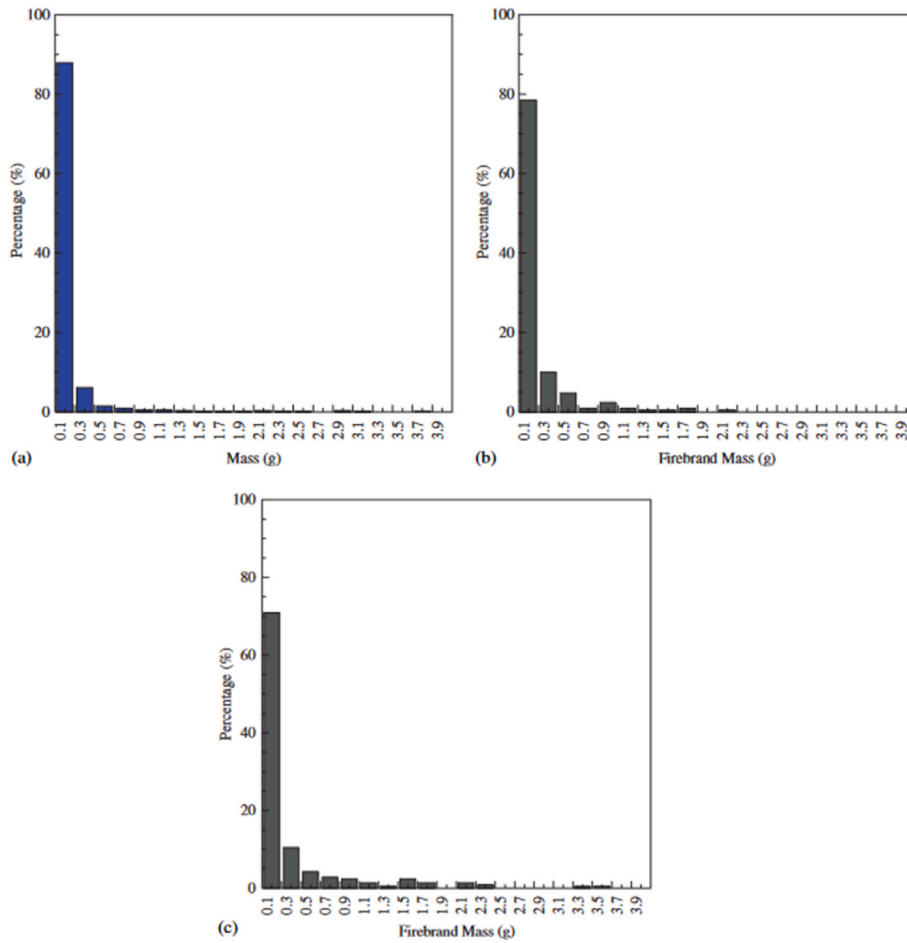
Fig. 4. Mass distribution of firebrands recovered from different trees: (a) 4.0 m Korean Pine, (b) 2.6 m Douglas Fir, (c) 5.2 m Douglas Fir. Taken from Manzello et al.[50]

$$Y_m = \left(\frac{3}{4}\left(\frac{C_D}{D_p}\right)\left(\frac{\rho_a}{\rho_s}\right)\frac{3.64}{g}\right)^{1.5} Z_c \tag{18}$$

where, D_p is particle diameter, ρ_s is particle density, Z_c is the height of Baum and McCaffrey's plume defined as

$$Z_c = \left(I_B / \left((\rho_a C_p T_0)\sqrt{g}\right)\right)^{2/5} \tag{19}$$

where, I_B is the fire heat release rate, C_p is specific heat of air, and T_0 is ambient temperature.

In the subsequent work, the authors extended this study for both firebrand propagation and lofting for the axisymmetric structural fires [68]. The authors developed the governing equations for the lofting,

combustion, and propagation of firebrands, which were tested for spherical shape particles. Woycheese and Pagni [69] developed three paradigms of combustion models for firebrand propagation and loftings, such as burning-droplet, linear regression and stagnation-point combustion. In the burning-droplet method, a crude first approximation of wooden brands was modelled for a spherical fuel particle combusting in an oxidising and quiescent atmosphere. The size of firebrand shapes can be determined from the constant linear regression model, which is very simple, but a good approximation was found with the literature data. The change in firebrand diameter with respect to time is $dD_p/dt = -E_r$, where E_r is the regression rate chosen for the material comprising the firebrand. The stagnation–point combustion model is useful for the disk type burning firebrands when the angle between the disk space and
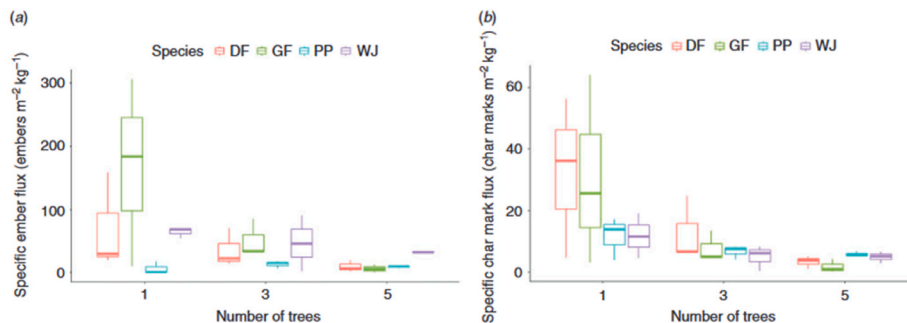

Fig. 5. (a) Specific firebrand flux and (b) Specific char-mark flux for each species, as measured by marks left on fire-resistant fabric panels. DF, Douglas Fir; GF, Grand Fir; PP, Ponderosa Pine; WJ, Western Juniper. Taken from Hudson et al. [74].

relative wind is 90°. The dimensionless propagation distances were determined for a range of initial thickness, ambient wind, and angle of attack. Woycheese and Pagni [69] reported large propagation distances for disk type wooden brands due to lift associated with 90 MW fire, which is much greater than that for spherical brands. In this study [69], disk is modelled with decreasing thickness, h and constant radius, R (representing decreasing mass, m). For an attack angle α, the disk lift (C_L) and drag coefficients (C_D) are $C_L = 1.17cos(\alpha)$ and $C_D = 1.17sin(\alpha)$, so that lift increases with decreasing α. Tohidi and Kaye [70] discussed that the largest plan area is always normal to the apparent wind leading the largest drag force but ignores lift forces. Woycheese and Pagni [69] did not explicitly mention this, instead mentioned that they used two attack angles i.e. angle between disk and wind = 35° and 90°. It is likely that 90° may correspond to the largest plan area being normal to the wind.

5. Benchmark experimental study

Firebrand generation and transport has also been investigated at a finer level of details with a variety of experimental studies. These studies can be separated into three groups based on their methodology: vegetation burning experiments, wind tunnel experiments, and firebrand dragon experiments. The first category is most suitable for firebrand generation. The other two categories are suitable for investigating different aspects of firebrand transport phenomena.

5.1. Vegetation burning experiments (firebrand generation)

Vegetation burning experiments provide valuable insight into firebrand generation, allowing researchers to investigate the effect of various factors (e.g. wind speed, FMC, size and species of vegetation) on firebrand generation under realistic conditions. In addition to this, landings of firebrands generated by burning vegetation can be captured shortly after generation and studied in detail, providing useful information about their physical and aerodynamic characteristics. Firebrand generation at the source can be quantified using this experimental data.

5.1.1. Firebrand collection indoor experiments

A series of common conifer tree species (Douglas-fir and Korean pine) burning experiments were conducted at the National Institute of Standard and Technology (NIST), USA to determine the mass and size distribution of firebrands while varying the FMC and tree height [50, 71]. Firebrands generated from the ignition were collected by placing water-filled pans at strategic locations around the tree base with no externally applied wind. The mass loss of the tree over time was recorded, along with the total mass of the collected firebrands. These data can be useful to quantify firebrand generation at the source using an inverse analysis (given in Section 7.3 of this paper).

According to the mass and size distribution data of firebrands, the majority lay below 0.3 g (as Fig. 4 illustrates). However, firebrands with 0.3 g mass can also cause ignition of a fuel bed as per Manzello et al. [72]. Firebrand surface area was calculated assuming cylindrical shape, with Korean pine found to produce firebrands with a larger surface area than Douglas fir. Larger surface area can lead to greater probability of secondary ignition.

The collected number of firebrands and the mass loss of the tree increased as the FMC decreased. It was reported that trees do not sustain burning when the FMC is more than 70% and the partially burning regimes occurred within the limits of 30%–70% [73]. A significant number of firebrands were generated when the FMC was below 30% in both tree species. The burnable mass consisted of needles and twigs, and the cylindrical firebrands were mainly composed of fragments of twigs. The needles did not produce firebrands and were consumed, contributing to the heat release.

For a similar FMC, the number of smaller firebrands collected from Korean pine was higher than the Douglas fir. Although both species produced smaller firebrands, a significant number of them burnt out in Douglas fir because of the higher heat release rate (HRR). This is explained by the fullness of the trees whereas the Korean pine shows sporadic burning and lower HRR because of the lower fullness of this species [50]. The heat produced by Korean pine may not be sufficient to consume smaller firebrands. When the tree size was increased the HRR also increased to consume more small firebrands, resulting in lower firebrands per unit mass of fuel consumption in taller trees [73].

5.1.2. Firebrand collection vs mass loss experiments - outdoor

Tree torching and firebrand collection experiments conducted at NIST were extended further by Hudson et al. [74] and Adusumilli et al. [75] at Oregon State University, USA. These experiments were conducted outdoors with four different species and focused on propensity to ignite spot fires as well as the size of embers and ember flux. In a series of experiments various vegetation such as Douglas fir, Grand-fir, Western Juniper, and Ponderosa pine with different heights (2.11 m–4.72 m) and fuel moisture contents (21%–40%) were burnt, placing an array of fire-resistant fabric panels instead of conventional water-filled trays to collect 'hot' firebrands. The landing of hot firebrands was determined as the landed particles would leave char marks on the fabrics. Maintaining a wind field of 1.2 m/s and burning 1 to 5 trees in order to vary the fire sizes of conducted tests were alternative approaches in these experiments in contrast to Manzello et al. [50,73] and Bahrani [76].

The highest median landed firebrand flux per kilogram of mass loss was recorded for Douglas fir trees (180 pcs/m^2/kg) and the highest hot firebrand flux was obtained from Grand-fir trees. The comparison with other species is shown in Fig. 5(a). The highest hot firebrand flux (at a landing location) per unit mass lost was Grand Fir. 30% of embers generated from Western Juniper were hot enough to leave char marks, giving it the highest char marks per fraction of total firebrands generated (Fig. 5(b)). This technique was further improved by Adusumilli et al. [75] increasing the number of firebrand collecting fabrics in the collection array. Douglas fir, Ponderosa Pine, and sagebrush vegetation with different heights and comparable moisture contents were ignited. The linear interpolation method was used to approximate the number of firebrands landing where fabrics were not placed, and the number of firebrands generated at the tree source was found by the linear extrapolation method. The linear regression model and coefficients for ember flux described in Hudson et al. [74] are presented in equation (20) and its associated Table 1:

$$EF^{1/3} = \beta_0 + \beta_1 MC + \beta_2 DBH + \beta_3 H*MC + \beta_4 DBH*H \qquad (20)$$

Based on the results of the experiments, the authors concluded that the total number of firebrands produced increases with the height of tree/shrub and the hot firebrand number exponentially increase with

Table 1

Coefficients for equation (20). MC is Moisture Content, DBH is Diameter at Breast Height, H is Tree Height.

Term	Estimate	s.e.	
$\widehat{\beta}_0 (intercept)$	5.99411	1.19823	***
$\widehat{\beta}_1 (MC)$	75.39059	16.75879	***
$\widehat{\beta}_2 (DBH)$	−0.43399	0.11927	***
$\widehat{\beta}_3 (H \times MC)$	−20.78155	4.49978	***
$\widehat{\beta}_4 (H \times DBH)$	0.11907	0.02985	***
$R^2_{adjusted}$	0.3848		***

Significance codes are: ***,0.001, **,0.01, *,0.05, .,0.1.

decreasing moisture content of vegetation species.

5.1.3. Firebrand collection experiments for various species as wind speed varies

Bahrani [76] conducted a series of vegetation burning experiments with a variety of species common to wildfire-prone areas of the US. These experiments investigated the effect of wind speed and vegetation type on the physical characteristics and landing distribution of firebrands generated by each of the selected species. The species chosen for these experiments were Little Bluestem Grass, Chamise, Saw Palmetto, Loblolly Pine, and Leyland Cypress.

The experimental setup was constructed in the wind tunnel facility of the IBHS (Insurance Institute for Business and Home Safety) Research Centre, USA where a 15 × 7 grid of 1.8 m diameter fans was set up to generate the desired wind profiles at a low, medium, and high wind speed. Downwind of the fans, a line burner was set up at the edge of the vegetation sample to be burned – in the case of shrubs, a bed of pine needles was laid between the burner and the vegetation to be burned. A set of 46 water-filled pans was placed downwind of the vegetation sample, organized in a dense grid close to the sample and spaced gradually further apart further downwind of the vegetation. Captured firebrands were dried in an oven at 103 °C for over 24 h before being weighed and measured via digital image analysis.

Bahrani used the dataset generated by these experiments to analyse several statistical trends in the overall distribution of firebrand masses and areas. 98% of captured firebrands were found to be under 1 g, and 88% had a projected area of less than 3 cm^2. For all species tested, firebrand mass was correlated with an increase in the projected area. The relationship between wind speed and firebrand mass was found to be highly varied, as shown in Fig. 6. Increasing wind speeds produced no clear trend in the number, mass, or projected area of captured firebrands. Wind speed was only found to consistently increase the flying distance of firebrands.

5.2. Wind tunnel experiments

Wind tunnel experiments allow for the most detailed study of firebrand transport, allowing for very precise control over the characteristics of the wind field and firebrands. Wind tunnel experiments are versatile and can be used to study several aspects of firebrand transport and landing, as well as the characteristics of firebrands in flight and how they change throughout the transport process.

These experiments can also be linked to the development of computational models of firebrand transport, such as in the case of
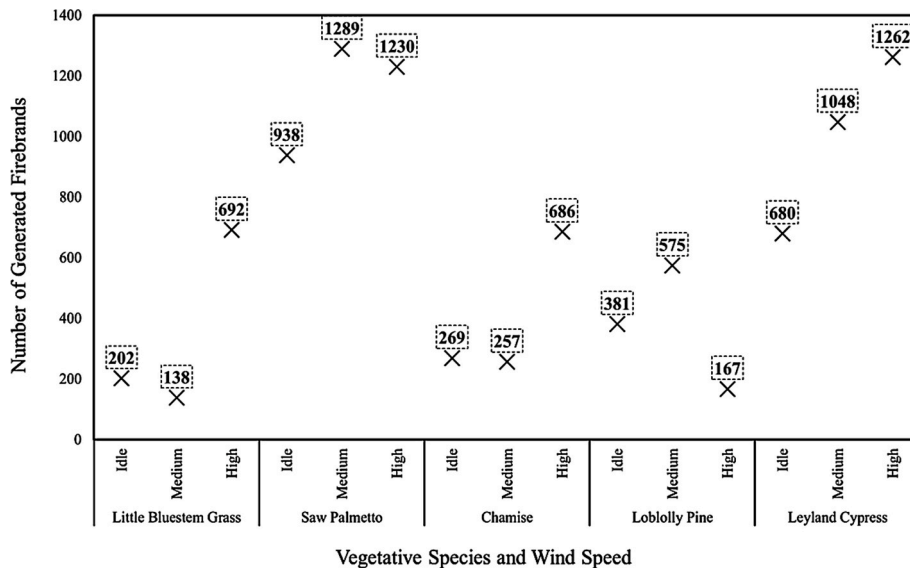

Fig. 6. Number of Firebrands generated by species under different wind conditions, from Bahrani [76].
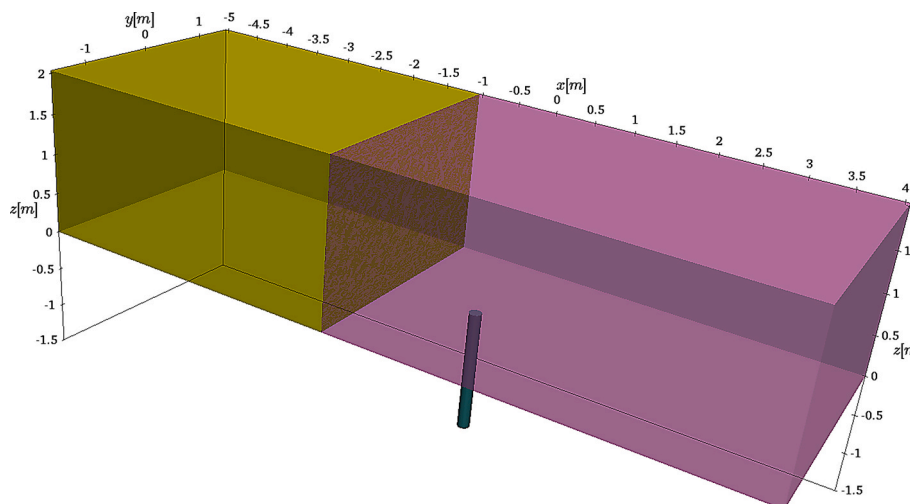

Fig. 7. Schematic of the wind tunnel experiment, showing dimensions and location of the pipe through which model firebrands were inserted.
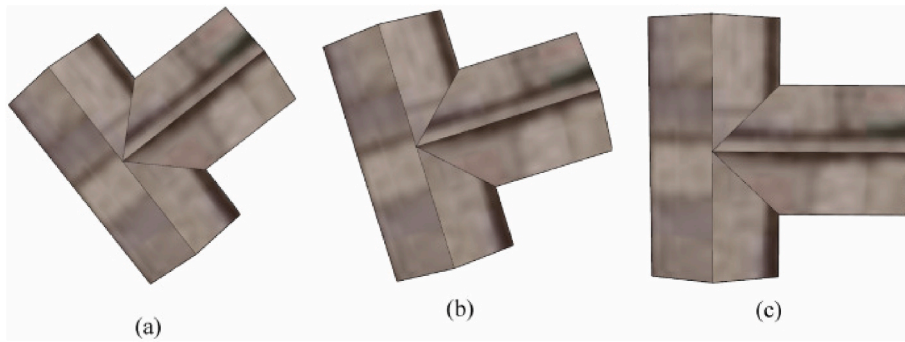
Fig. 8. An example of a T-shaped model structure used in these experiments, presented at three different angles: (a) 60°, (b) 75°, (c) 90°.

Tohidi's experiments at Clemson University [70]. In cases such as these, the experimental aspects of the study are discussed in this chapter, and the computational aspects are discussed in chapter 7.

### 5.2.1. Drag and spotting characteristics

Tarifa et al. [55,56] constructed two wind tunnels (horizontal and vertical) to measure the aerodynamic behaviour of firebrand particles at Instituto Nacional de Técnica Aeroespacial "Esteban Terradas", Madrid, Spain. In the horizontal wind tunnel apparatus, they used a two-component strain gauge balance to hang a firebrand particle to

study variation in the aerodynamic drag with the combustion of burning particles at different flow speeds. It was used to develop a correlation between aerodynamic drag with the mass of particles at different flow speeds. The vertical wind tunnel apparatus is used to study a similar aspect, however, firebrands were allowed to move freely during the combustion process.
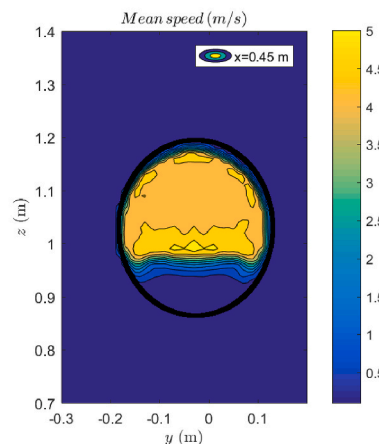
They developed multiple correlations between spotting behaviour such as flight time, maximum spotting distance with firebrand characteristics such as shape, size, aspect ratio, mass, and FMC. These are discussed earlier in Section 4.2 already. They observed that the flight
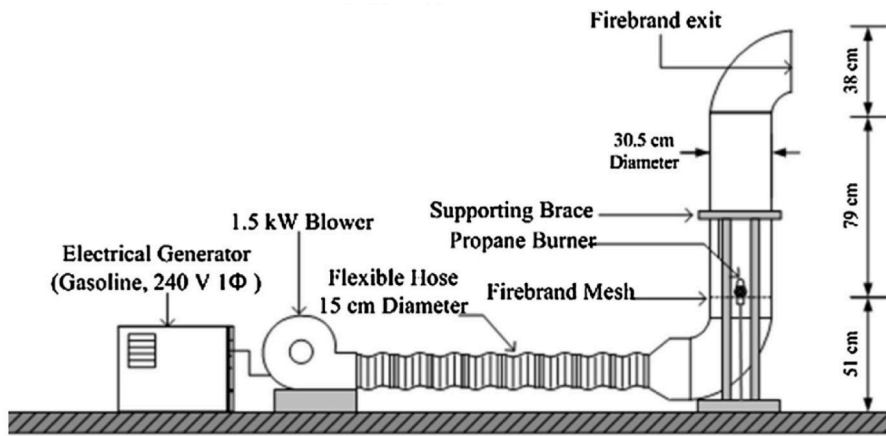
(a) NIST FD side view
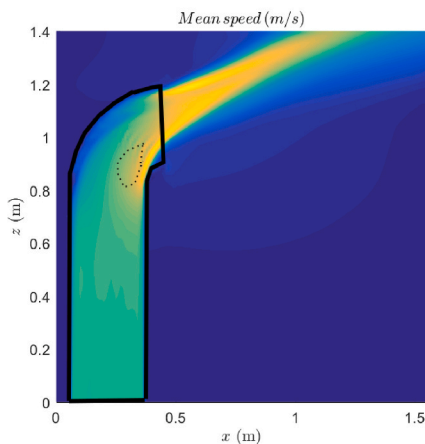
(b) Mean flow profile in the centreline XZ plane

(c) Mean flow profile in the YZ plane

Fig. 9. NIST FD schematic and CFD modelling of flow within it. (a) Schematic side view of NIST FD (taken from Manzello and Suzuki [81]); (b) and (c) CFD modelling of the end pipe section which highlights the formation of Dean's vortex which produces non-uniformity at the mouth (taken from Wadhwani et al. [88]).

paths of firebrand particles can be accurately computed by assuming that the firebrands fly at their final velocity of fall, a velocity that decreases continuously as the firebrand burns. They also found that the aerodynamic drag of a burning particle on which a constant airspeed flows acts as a function of time mainly because its size decreases as it burns. Furthermore, the aerodynamic drag coefficient may vary because of shape changes and due to the combustion process. From the results of their studies, it is possible to calculate the maximum range of possible fire spread by firebrands of given initial characteristics, if the convection column configuration and wind conditions are known. Fire spread by firebrands depends essentially on the convective currents and wind conditions in forest fires. Therefore, an accurate knowledge of these phenomena is absolutely required in order to correctly apply the information obtained from the basic studies on firebrands.

5.2.2. Bimodal distribution

Song et al. [77] conducted a wind tunnel experiment to study firebrand transport. The experiment is conducted on circular disk firebrands of three different sizes heated by a hot plate above the ground and driven by two different wind speeds. They observed a bimodal distribution (burning and extinction modes) for small firebrands under certain wind speeds. The firebrand transport distance and mass loss in the extinction mode are smaller than those in the burning model. A semi-empirical heat transfer analysis shows that there is a critical wind speed to quench the firebrand and produce a bimodal distribution, and its value increases with both the particle size and the heating duration. The semi-empirically predicted critical wind speed agrees well with experimental measurements.

5.2.3. Lofting behaviour

Tohidi and Kaye [70] conducted a series of wind tunnel experiments with the aim of examining the trajectory of model firebrands lofted into a wind field similar to those of firebrands lofted in the convective column of a wildfire.

In these experiments, a vertical pipe was inserted through the wind tunnel floor, and from the pipe model firebrand particles were injected with an initial upward velocity by an air jet into a well-characterized horizontal wind field (see Fig. 7 for an illustration of the wind tunnel and particle insertion location). Model firebrands were constructed of polyurethane and were cut to form rod-like particles of different length-to-width aspect ratios with square cross-section (η = 1, 4, and 6). The motion of particles travelling through this wind field was recorded by digital photography and analysed using image processing techniques to produce plots of individual particle trajectory and landing position.
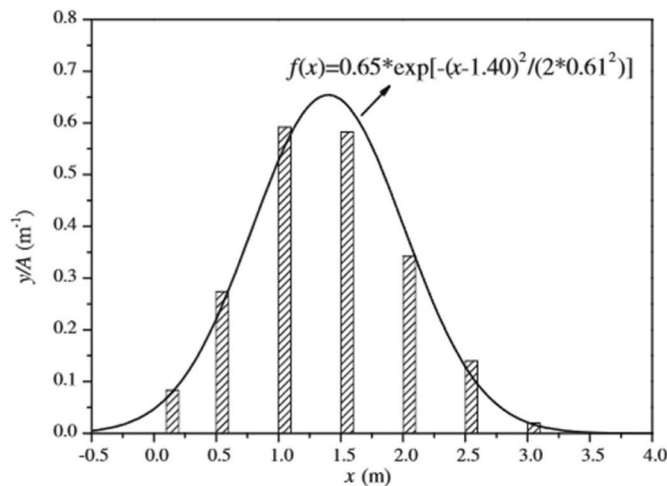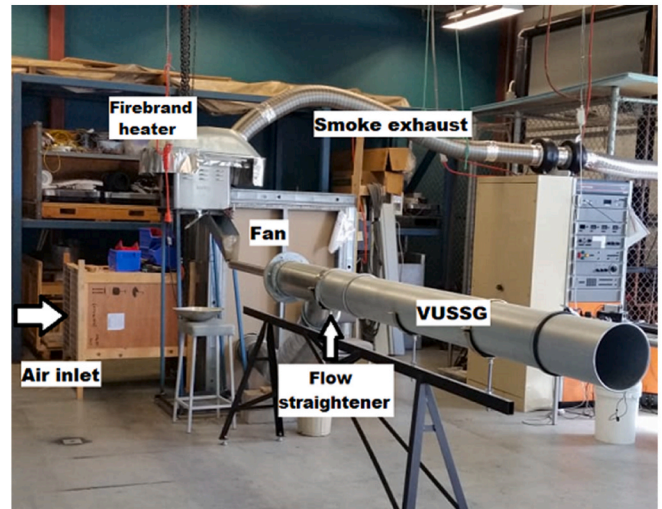

(a) Prototype plastic firebrand generator (non-burning firebrand only)

(b) Stainless steel firebrand generator (both burning and non-burning firebrand)

Fig. 11. Victoria University firebrand generators (taken from Wadhwani et al. [88,89]).

These experiments were repeated 200 times for each aspect ratio with three vertical and three horizontal wind speeds, producing a 3×3 array of trajectory plots for each aspect ratio.

These trajectory plots and firebrand landing positions were then analysed to obtain certain key information about firebrand transport under these conditions, such as maximum rise height during transport and probability density functions of downwind firebrand landing position.

While geometric and dynamic similarity to full-scale firebrand transport could not practically be obtained in these tests, the results still provide useful insight into the transport process – in particular, the results were used to develop and test the performance of a detailed computational model of firebrand transport (discussed in chapter 7).

5.2.4. Firebrand accumulation on model structures

Nguyen and Kaye [78,79] performed a number of wind tunnel experiments with the aim of investigating the accumulation of firebrands on structures. These experiments were conducted using a variety of 30:1 scale models of structures constructed with a range of ground footprints and roof geometries, such as those shown in Fig. 8. Model firebrands were created by pulverizing dried pine straw, which produced firebrands of approximately 10:1 scale relative to those found in field conditions. Each test consisted of a single model structure placed in a well-characterized wind field at a known angle to the direction of the wind. Model firebrands were then released into the wind field through an array of pipes in the ceiling of the tunnel. Once all model firebrands had been released, the wind was turned off, and the mass of firebrands spread across the roof surfaces was recorded. Wind speeds for these experiments were recorded as Tachikawa numbers (K), a dimensionless value that allows for comparison of results between scales. The Tachikawa number is defined as:

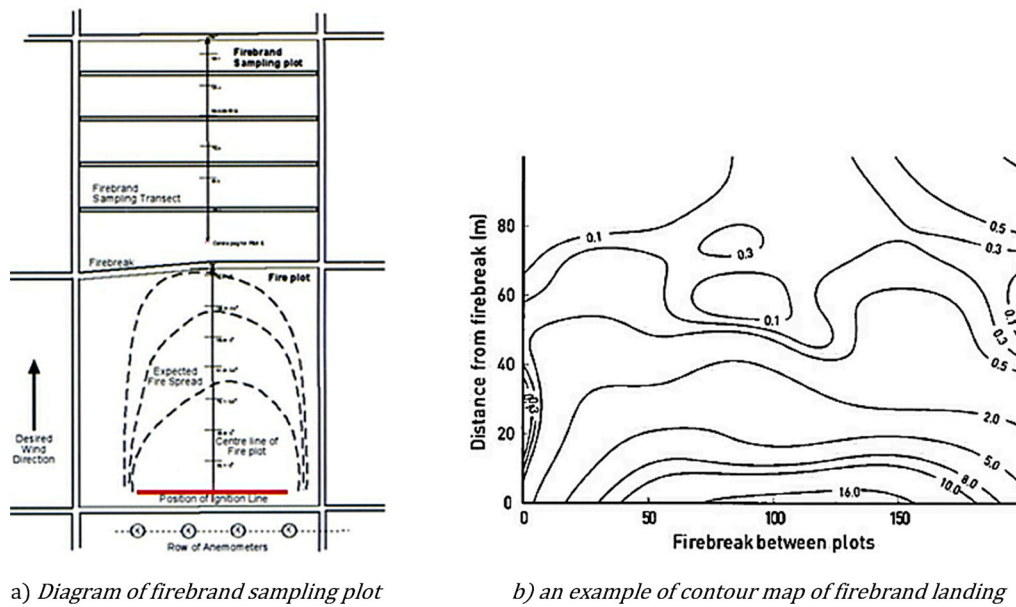$$K = \frac{\rho_a u_{ref}^2}{\rho_s g L} \tag{21}$$

Fig. 10. Gaussian distribution fitted to the number of firebrands per square meter at distance x.

a) *Diagram of firebrand sampling plot*   b) *an example of contour map of firebrand landing*

Fig. 12. Diagram of firebrand sampling plot and the observed distribution of firebrands [27].

where u_{ref} is the wind velocity measured at the height of the eave of the model and L is the mean ember diameter.

The observed mass accumulation of model firebrands showed that only a small fraction of firebrand mass that landed on a roof surface would remain on the roof for more than a short duration of time. Firebrands were observed to accumulate along the internal corners of certain roof geometries, where two surfaces met at an angle. When there were no corners available (such as in the case of a rectangular footprint building) only a negligible quantity of firebrands would remain on the roof. For geometries that had internal corners, both the angle and speed of wind incident on the roof had a significant impact on total mass deposited. Increased wind speeds tended to reduce the total mass deposited, while certain angles would create low-velocity flows over key areas of roof geometry that allowed firebrands to accumulate.

In addition to this, it was found that for a given roof geometry and incident wind angle there is a critical Tachikawa number (K_C) where particles of certain dimensions will not be able to land on the roof. Equivalently, there is a critical length L_C for a given rooftop geometry, wind speed, and angle, and particles of length less than L_C will not be deposited under those conditions.

5.3. Firebrand dragon experiments

Firebrand dragons allow for the production and transport of burning firebrand showers similar to those observed in field-scale occurrences, but in more controlled conditions. Firebrand dragon experiments are particularly useful for investigating the behaviour of firebrands landing on a surface, penetration of roofing material and accumulation on structures to name a few.

5.3.1. First firebrand dragon design - NIST, USA

Manzello from the NIST (National Institute of Standards and Technology) led the team in constructing a firebrand dragon (FD) that produces a controlled artificial shower of firebrands in a confined space. The NIST FD design and working details are discussed by Manzello et al. [80,81]. The firebrands can be loaded in NIST FD and burnt off with a propane burner flame, while a blower from the bottom provides the required uplift force to drive firebrands out from the bent shape (shown in Fig. 9(a)). NIST FD can be used to study spotting distance, and firebrand impact on full-scale structural material such as fencing, decking, wood joints, and roof tiles. However, in a wind tunnel facility, firebrands

are transported in a confined space to study impacts on scaled structures. NIST has a collaboration with the Building Research Institute (BRI) in Japan to utilise a large-scale wind tunnel with the NIST FD for firebrand transport.

The objective of the NIST FD is to simulate a wind-driven firebrand shower as observed in short and medium range spotting, rather than firebrand lofted by the convective column. The NIST FD has mainly been used to study the impact of firebrands on structures to understand firebrand penetration in roofing, vents, fences and decking [81–86]. The NIST FD is flexible enough to control the amount of firebrand density to understand firebrand release from a single tree or a forest as in WUI conditions. Some quantitative data of such firebrand release can be found in Section 5.1.

Zhou et al. [87] used previously obtained firebrand shape and mass information from the tree burning experiments [73] in the NIST dragon to study the transport of firebrands. Their study used cubiform, cylindrical, circular disk-shaped firebrands in different wind conditions to quantify the spotting distance of firebrands. Their work only discussed the longitudinal distribution of firebrands in the direction of the wind and they fitted the data with a Gaussian function (see Fig. 10); however, the distribution in the lateral direction is not provided.

Due to a 90° bend at the mouth, NIST FD is likely to produce non-uniformity in the wind flow. Wadhwani et al. [88] conducted a CFD analysis of the top pipe section of the NIST FD where a uniform inlet velocity was initialised as discussed by Manzello and Suzuki [81]. A uniform flow velocity of 3 m/s was initialised at the bottom of the modelled pipe. The CFD results showed a Dean's vortex was formed (highlighted by dotted lines in Fig. 9(b)) near the mouth of the NIST FD. Fig. 9(c) shows mean flow profile at the mouth showing non-uniformity. Such non-uniformity may not affect objectives of the experimental studies conducted with NIST FD. However, firebrand transport scenarios studied by a firebrand generator with uniform flow are easier to simulate with CFD models.

5.3.2. Two concentric pipe firebrand generators

Wadhwani et al. [88,89] constructed firebrand generators using two concentric pipes to produce a uniform flow of firebrand particles. The objective of their firebrand generator was to produce firebrand particles that were used to validate and improve the Lagrangian particle sub-model of Fire Dynamics Simulator (FDS). Wadhwani et al. [88] have discussed the design and construction of the prototype firebrand
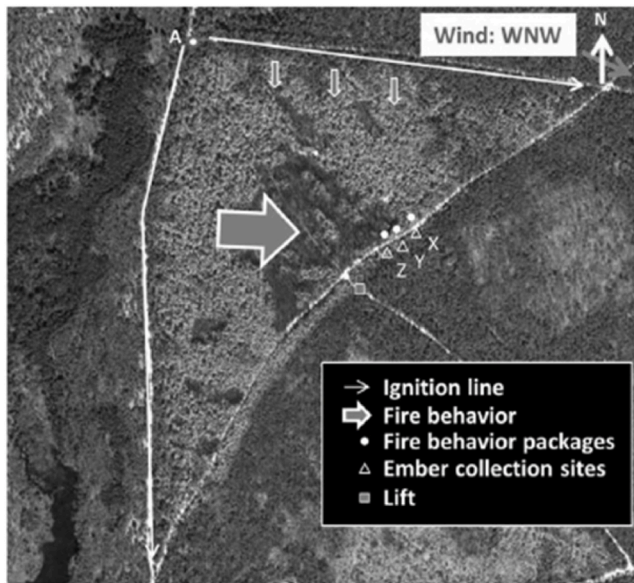
Fig. 13. A post-fire satellite image of the Pinelands National Reserve (PNR) burning plot in 2016 prescribed fire. The X, Y, Z firebrand collection sites (FCS) are represented by triangle that are located at the right side of the road. Fire Behaviour Packages (FBP) represented by dots are established on the left side of the road opposite the FCSs. The wind direction is WNW (taken from Filkov et al. [10]).

generator (made of plastic) used to study the transport of non-burning cubiform and cylindrical firebrand particles. The stainless steel generator (dubbed as VUSSG) is quite similar to their prototype, however, it can produce different flow Reynolds numbers and can accommodate burning or partial burning firebrands [88,89]. Both generators are shown in Fig. 11.

Wadhwani [88,89] measured velocity profiles, particle velocities and particle distribution of the mouths (firebrand outlets) of both generators and used them as the input parameters for transport modelling using FDS. He also measured landing distributions of burning and non-burning firebrands on a gridded surface to quantify the suitability of the FDS Langrangian particle sub-model.

5.3.3. Vertically feeding firebrand shower in wind tunnel

To study convective plume driven firebrand transport using NIST FD, the FD exit mouth needs to be oriented upward and the FD needs to be placed in a wind-tunnel or under the influence of ambient wind. However, Hashempour [90] noticed strong reverse flow within the FD in such configuration. To avoid this, he constructed an ember shower simulator (ESS) that creates an artificial firebrand shower vertically. The design consists of a wind tunnel which includes an inlet duct, a contractor and a test section with a firebrand generator mounted below the wind tunnel. The fan blows air into the wind tunnel, and the air passes through the contractor before entering the test section (for detailed design and working see Hashempour [90]). However, the design eventually produced a wind-driven firebrand shower. Hashempour & Sharifian [91,92] used ESS to test the standard firebrand guard meshes that are being used for protection purposes against the firebrand shower of firebrands with an average projected area of firebrand from 2.5 to 16 mm^2.

Hashempour [90] observed two mechanisms of firebrands passing through the screens (firebrand guard). Some firebrands shatter into smaller firebrands which were called secondary firebrands and then passed the screen opening. Some other firebrands, that were less vulnerable, keep burning behind the screen to reduce their size and pass through the screen opening. He observed that the combination of the buffer zone between firebrand screen guard, fuel, and screen remarkably reduced the number and size of firebrands on the fuel bed.

6. Field-scale experimental study

To the best of the authors' knowledge, only two field studies have been carried out to quantify firebrand spotting, Project Vesta [27] and Filkov et al. [10,48,93].

6.1. Project Vesta, Australia

Project Vesta [27] was a project by the CSIRO to develop an improved model of fire propagation in Eucalypt forests. This project involved detailed measurements of multiple significant factors that impact fire propagation in field-scale burning experiments. These measurements include detailed profiles of fuel load and distribution at several heights within the forest, wind profiles, fuel moisture content, and firebrand landing densities downwind of the fire front.

The experimental setup of this field-scale study consisted of multiple 200×200 m plots of eucalypt forest at two different sites ("blocks") in Western Australia – the McCorkhill Block and the Dee Vee Block. Each of these sites offered different fuel distributions and ages, McCorkhill having a dense layer of shrub beneath the canopy, and Dee Vee having a sparse understorey. At each of these sites, different plot areas were selected based on the age of fuel in the plot.

For a selection of plots in this study, an area downwind of the plot was set up to measure the distribution of firebrands. A series of large plastic sheets were laid out on cleared areas of ground perpendicular to the direction of the wind. Firebrands that landed on the plastic sheets would leave a clearly identifiable burn mark or hole, allowing for accurate measurement of firebrand landing density over the area of the sheet. Short-distance spotting was recorded by researchers tagging individual spot fires as they occurred. A row of anemometers were placed upwind of the ignition line (see Fig. 12a) to measure the wind velocity.

After detailed data on fuel load, moisture content, and sub-canopy wind speeds were recorded, each plot was burned by igniting a 120 m line at the upwind edge using drip torches. Firebrand distribution data was analysed for four cases. These distributions were plotted as contour maps (an example is shown in Fig. 12b) and analysed.

Based on these analyses, Project Vesta found that firebrand distribution parallel to the wind can be approximated as an exponential function and distribution perpendicular to the wind as a normal distribution. Landing density downwind of the fire is approximated by:

$$D_{fb} = D_0 e^{-a_3 d} \tag{22}$$

where D_{fb} is firebrand landing density at a given distance d downwind of the fire, D_0 is firebrand landing density at the edge of the fire, and a_3 is a constant.

For distribution along a transect perpendicular to the wind, the landing density is approximated by:

$$D_{fb} = D_{max} e^{-\left(\left(d - d_{max}\right)^2\right)/c_3} \tag{23}$$

where, D_{max} is the maximum landing density that occurs at a distance d_{max}, and c_3 is a constant.

Fuel age was found to significantly increase the number of firebrands generated, closely corresponding with the observed change in bark thickness with age. Short-distance spotting (up to 50 m) was found to occur first as a near-simultaneous ignition of multiple fires shortly after the fires reached a firebreak, followed by intermittent spot fires for some time afterwards. Longer-distance spotfires were observed out to a distance of up to 1145 m, but typically landed within approximately 250 m of the fire front and were considerably less frequent than spot fires within 50 m. A provisional model of firebrand distribution was developed from this analysis using the parameters of predicted fire rate of spread, fuel hazard score, and above-canopy wind speed as a series of

tables. These tables are given in Appendix VIII of the Project Vesta report [22].

6.2. Pineland National Reserve (PNR) in new Jersey, USA

A series of prescribed forest fire experiments were conducted in Pineland National Reserve (PNR) in New Jersey in the USA from 2013 to 2016 (a burnable plot is shown in Fig. 13) [10,48,93] to quantify the characteristics and flux of firebrands during the management-scale wildfires. Thermal image recording and video footage analysis were also used to measure the firebrand velocity, size, number, and firebrand shower durations at the particle collection plots [10].

More than 70% of firebrands were found as bark slices and the remaining were shrubs and the branches of pine. Most of the firebrands' mass lay between 5 and 50 mg while 30% of them were 10–20 mg [10]. The majority of firebrands had the size of $(5\text{-}20) \times 10^{-5} \text{ m}^2$ that has a good agreement with the real fires such as Angora [49,72]. The number of firebrands decreased with increasing firebrand area similar to the single tree burning experiments of Manzello et al. [50]. The measured velocity of firebrands ranged 0.1–10.5 m/s with an average of 2.5 m/s [10] under the influence of wind. Processing of thermal image recording showed that the firebrand particles in the airflow increased in number up to 180 pcs/s [10] in a 1 m^3 control volume starting from a distance of 13 m ahead of the fire front.

It was found that the temporal and spatial variations of firebrand fluxes were directly linked to the intensity of the fire that was measured based on the surface fuel consumption in the experiment of 2016 [93]. The averaged wind velocity (1.4 ± 0.6 m/s) and the ambient temperature (13 °C) of the environment were monitored at a meteorological station located at the burning plot as the experiment proceeded. The firebrands were collected at three firebrand collection centres (FCS) in the downwind region where location specified fluxes were recorded as 0.82, 0.9, 1.36 pcs/m^2/s for the fire intensities ranged from 7.35 ± 3.48 MW/m to 12.59 ± 5.87 MW/m [93]. Firebrand flux was positively correlated with the higher fire intensity and shorter distances from the fire front and vice versa. As per visual observations coupled to the local fire behaviour measurements show that firebrand showers occurred up to 100 m ahead of the fire front at collection sites for a certain time interval depending on the movement of fire at a yield spread rate of 0.289 m/s [93].

The firebrand size distribution results show the majority of firebrands are less than 30 $\times 10^{-5} \text{ m}^2$. The percentage reduction of smaller firebrands ($<20 \times 10^{-5} \text{ m}^2$) is relatively consistent with the increase of separation distance and considerably varies for larger firebrands [93].

7. Computational fluid dynamics (CFD) simulations

The Computational Fluid Dynamics (CFD) simulations are recognized as viable alternatives to studying firebrands experimentally. These simulations facilitate overcoming the limitations of financial resources, human resources, safety precautions, and the requirement of advanced technologies to conduct laboratory-scale and field-scale experiments. A number of open-source and commercial models are being used, of which some models have been validated with a range of experimental studies. There are multiple studies conducted by CFD modelling to understand the physics of the key processes of firebrand behaviour. Some of them have focused on a single aspect while others considered multiple aspects of firebrand behaviour.

Firebrands are considered point particle or spherical shapes in Tarifa et al. [59] model (Section 4.2) and Albini model [47] (Section 4.3), however, in real fires irregular shapes occur, not necessarily ideal shapes as assumed. CFD-based fire models solve an approximate form of the Navier-Stokes equation with a low-Mach number approximation. Most of the firebrands observed in real fire are generally irregular-shaped, rod-shaped or disk-shaped [10,48,81,94]. Thus, their aerodynamic behaviour would be different from the previously assumed ideal-shaped

firebrands. CFD-based models account for the shape of firebrand particles along with the combustion parameters such as described in Woycheese and Pagani [69]. They studied the transport of disk-shaped firebrands in 2D convective plume which considered the effect of firebrand shape in the spotting behaviour of firebrands. This section highlights the significance of firebrand modelling addressing the type of the source code (commercial and institutional code, in-house code), transport mechanism (fire, plume, and wind), and state of firebrands (ambient temperature, hot, or burning).

7.1. Commercial and institutional codes

Out of many developed CFD codes, some are freely available to use and others are served for commercial purposes or institutional research. FDS [95] is an open-source code developed by the National Institute of Standards and Technology (NIST), USA while ANSYS [96,97] is a commercial code that is widely used in firebrand modelling. Institutional codes such as Weather Research and Forecasting (WRF) [98] are used to spin up turbulent boundary layers by Large Eddy Model (LEM) to facilitate firebrand transport in some studies. As a product of Los Alamos National Laboratory (LANL), HIGRAD/FIRETEC institutional code is used to model coupled interaction between fire, fuels, atmosphere and topography to include firebrand dynamics [99]. The applications of such commercial and institutional codes to investigate firebrands' spotting and the effect of the state of particles are discussed in detail in sections 7.1.1 to 7.1.3.

7.1.1. Firebrands transported by fire buoyancy

In this subsection, studies are reviewed where combustion is modelled. It may be through specifying a HRR or pyrolysis rate (PR) where HRR = PR x heat of combustion, or modelling the pyrolysis process followed by modelling a chemical reaction between pyrolyzed fuel and oxygen. The inclusion of combustion processes generates more realistic turbulence around firebrands.

Koo et al. [99] carried out physics-based coupled fire modelling for the transport of cylindrical and disk-shaped firebrands. In this model, the wind field is generated using HIGRAD/FIRETEC [100] combined with the wildfire model developed by the LANL to provide turbulence including detailed wind flow for firebrand transport. The drag and lift forces on the firebrands are calculated based on the particle geometry, relative wind velocity and combustion. They carried out two broad sets of simulations representing surface fire only and another representing crown fire including the surface fire. The spot ignition hazard was evaluated and found disc shape firebrands travel further than cylinders as discs are aerodynamically more favourable. The disk-shaped firebrands have larger drag/weight ratio when their attack angle (angle between axis of particle and wind) is assumed to be 90° which assisted in developing higher buoyant force for farther travel. The travel distance of firebrands generated from canopy fires is found larger than the firebrands coming out from surface fires by this study.

Wadhwani et al. [101] carried out a parametric study for the transport of firebrands inside a forest canopy using a physics-based fire model, FDS. The objective of their work is to showcase the capability of their validated fire model to understand the dispersion of short-range firebrands inside an idealised forest. They explored the effect of firebrand characteristics (shape, size, initial temperature, and initial height) and fire intensity on firebrand distribution. The streamwise distribution of firebrands was observed and found qualitatively similar to the field measurement/observation for short-range spotting carried out for Eucalyptus vegetation [27,102] and Pine plantation [93]. The sphericity and mass of firebrands critically affect the landing distribution in the streamwise and crosswise directions. For approximately the same mass, a firebrand with a lower value of sphericity travelled farthest in the streamwise direction and dispersed more in the crosswise direction. The maximum spotting distance (within which 95% firebrands land) and the dispersion of the firebrands in the crosswise direction are also

significantly affected by the sphericity and mass of the firebrand. The spotting parameters, such as median of spotting, first and third quartiles, and maximum spotting distance in streamwise and crosswise directions, are found to increase with the intensity of the surface fire. The firebrand's initial temperature is found to have minimal impact on firebrands which remained inside the forest canopy. However, its effect on firebrands which travelled beyond the forest canopy is inconsistent with the initial temperature. The initial height of the firebrand appears significant to the final firebrand distribution. In almost all cases, the firebrands released from the trunk region travel a shorter distance than the firebrands released from the crown region.

Wickramasinghe et al. [103] numerically estimated the firebrand generation rate through inverse analysis using FDS from a Pitch Pine forest burning following the field experiment conducted by Thomas et al. [93]. The fire intensity was prescribed while maintaining the environmental conditions such as average wind speed, relative humidity, and ambient temperature same as the experiment. The fuel load and the characteristics of Pitch Pine Forest (tree height, dimensions of vegetation particles) were modelled. The firebrand landing flux at the downwind of the fire was reasonably matched with the experiment by trial and error. The firebrand generation rate was found as 4.18 pcs/MW/s (pcs-pieces) - correlated to the fire intensity by this technique.

Following the numerical study of Sardoy et al. [104,105], firebrands combustion was investigated by Menzemer et al. [106] accounting for the changes in size, shape, and the flow dynamics around the particles during transport using FDS. The potential of starting an ignition was categorized based on the state of firebrands which are flaming, smouldering, inert hot and inert cold. The pyrolyzing of firebrands was modelled considering the Arrhenius equation's first-order reaction rate in this study. The firebrands exposed to higher temperatures were fully pyrolyzed during first few seconds, while the firebrands that were exposed to lower temperatures remained intact for a longer time showing lower cooling rates. Depending on the product of firebrand initial density (ρ_f^{w0}) and the thickness (τ), the dynamics of firebrands lifting by the plume was also determined in this study. It was found that when $\rho_f^{w0} \times \tau \geq 1$, the firebrands do not lift and $\rho_f^{w0} \times \tau \leq 0.6$ resulted in particles lifting and travel at least 50 m from the fire.

7.1.2. Firebrands transported by plume

Focusing on the simplicity of the models, some studies used a plume instead of a fire to create the necessary buoyancy to lift firebrands and subsequently to transport blending with the horizontal wind. The firebrand terminal velocity is examined for long-range spotting by Thomas et al. [98] using combinations of codes. The WRF atmospheric model was used in LEM to simulate the turbulent boundary layer and a plume was introduced by modifying the WRF-Fire code. The constant terminal velocity and the variable terminal velocity were investigated and found that either version overestimated the firebrand landing density compared to simulations in which the terminal-velocity assumption is not made.

7.1.3. Firebrands transported by wind only

Wadhwani et al. [107] used two firebrand generators (shown in Section 5.3.2) to study the transport of non-burning cubiform, cylindrical and square-disc firebrands and used only cubiform firebrands as burning firebrands. They observed that FDS [95] is capable of estimating firebrand distribution and could reproduce experimental findings. It was found that using general shape-dependent drag models (such as Haider and Levenspiel drag model [108]) could produce comparatively similar or better peak location of landing contours and longitudinal distribution of firebrands with the experiment than using inbuilt drag models of FDS which are applicable only for two shapes (spherical and cylindrical) [89]. Furthermore, it was also observed that the lateral distribution could not be improved as the point particle assumption of FDS restricted

the secondary motion (rotational motion) of the particle which significantly contributed to dispersion.

7.2. In-house codes

The governing equations of fire-driven fluid flows and dynamics of firebrands are solved by specific solving techniques such as Runge-Kutta [109] method or Euler scheme [110] presented as in-house codes in some studies. The OpenFOAM libraries [111] and UK Met Office LEM [112] are used in some simulations to examine the behaviour of firebrands in different transport mechanisms. The investigations conducted by in-house codes focusing on firebrand transport and their state are presented in detail in sections 7.2.1 to 7.2.2.

7.2.1. Firebrands transported by fire buoyancy

Like subsection 7.1.1, in this subsection, studies are reviewed where combustion was modelled. However, in these studies in house codes were used.

Sardoy et al. [105] investigated the combustion and dispersion of firebrands from burning trees numerically. A three-dimensional (3D) CFD model is used to precompute the steady-state gaseous flow and thermal fields induced by a crown fire into which firebrands are injected. The conservation equations are solved using the finite volume method with a second-order backward Euler scheme for time integration. The different approaches such as second-order central difference scheme, ULTRASHARP, PISO algorithm, and tridiagonal matrix algorithm (TDMA) were used to solve the diffusion term, convective term, pressure-velocity term, and resulting linear algebraic equations for each variable respectively. According to the outcomes of this study, the product of firebrand initial density (ρ_f^{w0}) and the thickness (τ) determines the shorter and longer distance landing. It is found that most of the firebrands landed at a shorter distance frequently showed a flaming state while the firebrands landed at a longer distance showed a charring state. It concludes that shorter distance firebrands pose a higher fire danger because of the flaming state and the high remaining mass at the impact.

7.2.2. Firebrand transported by plume

In this subsection, like subsection 7.1.2, studies are reviewed where no combustion was modelled. Instead, buoyancy is generated by using a hot plume. As subsection 7.2.1, in these studies in-house codes were used.

Himoto and Tanaka [94] used large-eddy simulation (LES) to simulate the transport of disk-shaped firebrands in a 3D convective plume. They modelled the lofting of firebrands from the ground with the convective plume and transported them with the turbulent boundary layer ahead of the plume. In their model, the maximum height a firebrand can achieve is described as a function of HRR, the density of air and firebrand, ambient temperature, and the width of the particle. Similarly, streamwise travel distance is derived with driving wind velocity, maximum height, and the heat source. Their numerical results were generalised reasonably well with a new non-dimensional parameter (B^*) (Eq. (27)). In their modelling, the maximum height (Y_m) (m) firebrand achieved is described as,

$$Y_m \cong \left(\frac{\dot{Q}}{\rho_a C_p T_o g^{\frac{1}{2}} D_p^{\frac{5}{2}}} \right) \left(\frac{\rho_a}{\rho_s} \right) D_p \tag{24}$$

where $\dot{Q}$ is HRR of surface fire (kW), ρ_a, ρ_s are the density of air and firebrand (kg/m³), T_o is ambient temperature (K), D_p is the width of the disk particle.

Moreover, streamwise travel distance (x'_p) (m) from the maximum height

$$x_p' = \sqrt{2}\left\{\frac{U_\infty}{(gD_p)^{\frac{1}{2}}}\left(\frac{\rho_s}{\rho_a}\right)^{-3/4}\left(\frac{\dot{Q}}{\rho_a C_p T_o g^{\frac{1}{2}}D_p^{5/2}}\right)^{\frac{1}{2}}\right\}D_p \tag{25}$$

here U_∞ is reference ambient velocity (m/s). x_p' is the distance only from the maximum height not the complete distance from the source of the fire. However, X_m represents the total distance of spotting, and correlated with x_p' as some functional correlation,

$$X_m = f\left(x_p'\right) \tag{26}$$

normalising Eq. (26) with initial height of firebrand above the ground (h_o) as the characteristic length scale to define the dimensionless parameter (B^*),

$$B^* = \left\{\frac{U_\infty}{(gD_p)^{\frac{1}{2}}}\left(\frac{\rho_s}{\rho_a}\right)^{-3/4}\left(\frac{\dot{Q}}{\rho_a C_p T_o g^{\frac{1}{2}}h_o^{5/2}}\right)^{\frac{1}{2}}\left(\frac{D_p}{h_o}\right)^{-3/4}\right\} \tag{27}$$

Thus,

$$\frac{X_m}{h_o} = f(B^*) \tag{28}$$

Moreover, they developed the firebrand distribution in the form of scattering distribution function in the x-direction as $p(x)$,

$$p(x) = \frac{1}{\sqrt{2\pi}\sigma_{L,x}x}\exp\left\{-\frac{(lnx - \mu_{L,x})^2}{2\sigma_{L,x}^2}\right\} (0 < x < \infty) \tag{29}$$

with x as the streamwise travel distance and $\mu_{L,x}$ and $\sigma_{L,x}$ are the mean and standard deviation of $ln(x)$. These are calculated with μ_x and σ_x (mean and standard deviation of x):

$$\mu_{L,x} = ln\frac{\mu_x}{\sqrt{1 + \left(\sigma_x/\mu_x\right)^2}}\sigma_{L,x} = \sqrt{ln\left(1 + \left(\sigma_x/\mu_x\right)^2\right)}, \tag{30}$$

Finally,

$$\mu_x/h_o = 0.47B^{*2/3}\sigma_x/h_o = 0.88B^{*1/3}, \tag{31}$$

$$\mu_y/h_o = 0\sigma_y/h_o = 0.92. \tag{32}$$

The scattering distribution function in the y-direction as $q(y)$,

$$q(y) = \frac{1}{\sqrt{2\pi}\sigma_y}\exp\left(-\frac{(y - \mu_y)^2}{2\sigma_y^2}\right) (-\infty < y < \infty). \tag{33}$$

with a new non-dimensional parameter with a characteristics length scale which is the initial height of the firebrand above the ground. This study can be expanded to include the phenomenon of change of firebrand mass, shape, or aerodynamic coefficients due to firebrand combustion.

The firebrand lofting, propagation and deposition were investigated by Bhutia et al. [113] in a classical 2D plume model and also in an LES-based 3D coupled fire-atmosphere model. The firebrands were released from a moving grassfire that was developed with coupled atmospheric-wildfire induced circulations. For both non-combusting and combusting particles, the motion of spherical particles was derived based on drag and gravity forces. The firebrand trajectory path was then decomposed into x, y, and z directions by including external forces and integrated numerically using a fourth-order Runge-Kutta method. The comparison of spotting distance obtained by classical plume model and coupled fire-atmosphere LES show a significant difference in this study. It was found that the higher the release height of firebrands, the longer the spotting distance. The downwind motion of the firebrands mainly depends on the mean wind component and the lateral motion by the fire-induced fluctuations. Further, the results revealed the burning firebrands fall faster than the non-burning firebrands and the differences in the trajectories also significant.

A coupled fire-atmosphere LES simulation was applied by Pereira et al. [114] for studying the maximum spotting distances for spherical shaped firebrands with a wide range of sizes. An equivalent volumetric heat source was used in the idealised forest fire from which the Lagrangian points representing spherical firebrands were released randomly. The firebrand transport model was defined by a system of differential equations assuming only drag and gravity contribute to the motion of point particles. Further assumptions were made for the volume of particles, which remain constant during drying and pyrolysis processes, while particle density also remains constant during char combustion. The Arrhenius equation was applied for the rates of mass loss due to drying and pyrolysis processes. The unsteady form of the momentum, energy and scalar concentration equations was used for the discretized domain with a finite volume method. The spotting distances obtained for different fire intensities were compared with the maximum distances obtained by the Albini model [44]. They found the spotting distances for a 2000 kW/m short grass fire compared satisfactorily with the Albini model and underpredicted by 40% for a higher intensity 50000 kW/m fire. There are significant assumptions made in the simulation that can be improved. The adoption of unsteady fire structure can make simulation more realistic, while the particle drag, and spherical shape assumption may be improved.

After completing the experiments referred to in Section 5.2.3, Tohidi and Kaye [111] ran simulations with the same initial conditions with a 3D six-degree of freedom firebrand transport model in OpenFOAM. The velocity field of the plume in non-uniform cross-flow boundary layers is resolved by time-varying LES simulations in this model. It was found that the developed model could predict the first and second order statistics of the flight of firebrands in relation to the experimental data.

Anthenien et al. [115] extended the work of Tse and & Fernandez-Pello [109] for wooden firebrands with different shapes such as the cylindrical, disk, and spherical that were lofted or released from a certain height in a buoyant plume. They simulated firebrand transport considering different terrain and wind conditions. Their study showed that for firebrands of equal initial mass, disks travelled the farthest and had the highest remaining mass fraction upon impacting the ground. While, spheres are carried the shortest distance, and cylinders have the smallest mass fraction upon impact. They also observed that higher surface burning temperatures are found to lead to a shorter propagation distance.

Thurston et al. [112] carried out a long-range spotting simulation with the in-house code of UK Met Office LEM for firebrand particles falling at their terminal speed to study the effects of turbulent plume dynamics on spotting patterns both in the lateral and longitudinal direction. Their study focused on understanding the dynamics of buoyant plumes generated by a surface fire to transport firebrands from a certain height. They assumed that the firebrands are released from 50 m above the ground (which is their first grid cell) which represents a high fire intensity scenario with aerodynamically efficient firebrand production. The above assumption is valid from the computational resource and hence surface fire, and the sub-grid wind are not fully resolved, and firebrands are assumed to fall with the terminal velocity. Their study showed that turbulent plume dynamics have a noticeable impact on the maximum spotting distance and the amount of spread (lateral and longitudinal direction) in the firebrand landing position. In-plume turbulence causes much of this spread and can increase the maximum spotting distance by a factor of more than two over that in a plume without turbulence in their simulation.

7.2.3. Firebrand transported by wind only

Tse & Fernandez-Pello [109] carried out numerical modelling for copper and aluminium-based metal firebrands releasing from power cables, and wooden firebrand particles coming from a tree. The work
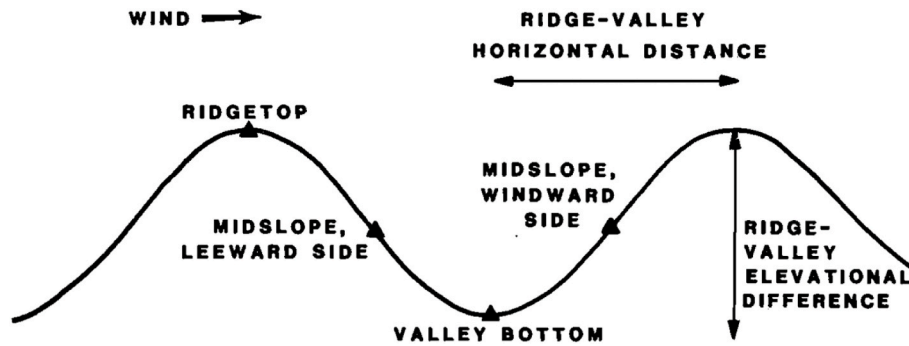
Fig. 14. Mountainous terrain and spotting source location for the maximum spotting distance model in BEHAVEPLUS (taken from Ref. [119].

focused on understanding the firebrand trajectory ejected at a certain height from the ground in the surface layer flow (30–50 m from the ground) and their potential to cause spotting. They solved the coupled ordinary differential equation representing mass, energy and momentum conservation using a Runge-Kutta method [116]. According to the results, the wooden firebrands fly the greatest distance followed by aluminium and copper particles under the same wind conditions. The wooden firebrands burn heterogeneously and can land in a still-burning state. However, metallic firebrands carry more heat than the wooden counterparts claiming a higher potential to start an ignition as found in this work.

Kortas et al. [110] carried out a 2D numerical approach for firebrand transport by solving a set of partial differential equations using the Euler scheme. The integration process of equations is continued to determine the horizontal and vertical velocities of firebrands to find the travel distances, mass, and diameter variations of firebrands due to pyrolysis. However, the work utilises random initial conditions for firebrand which uses the probability distribution function deduced from the experiment of Manzello et al. [80] as input value which could be the reason for acceptable agreement with the experiments. It is to be noted that firebrand flight is 3D and the 2D assumption is used in this study. They compared only longitudinal distribution against the experimental result for glowing cylindrical and circular disk firebrands published by Manzello et al. [80] using the NIST FD. Their observation was not compared against the lateral distribution (which is significantly important for non-spherical firebrand particles) which suggests the further simplification of simulation compared to the experimental setting.

7.3. Strengths and weaknesses of computational models of firebrands

The models described in sections 7.1 to 7.2 broadly explain the importance of one or a few parameters of firebrand behaviour under different fire-weather conditions. The reliability of some of these models [88,96,103,107] has been exhibited through validation against experiments. The ability to simulate many events controlling different parameters is an advantage of these CFD models. However, still, there is space for an integrated system with the completeness of firebrand generation; transport by fire-induced buoyancy and the driving wind; deposition/landing and secondary ignition due to the heat transfer between firebrands and landed surface. The least discussed aspects such as the interactions between the firebrands in a cluster of particles, the effect of irregular geometry and the rotational movements of particles for transporting, firebrand breakage from vegetation and combustion processes with accurate thermo-physical properties are also needed to examine in depth. The changes of mass and the shape of firebrands due to combustion and pyrolysis during flight cause variations of instant resultant forces exerted on them. This leads to changing their trajectories and spotting distance and as some studies [94,105,114] used, as the assumption of constant mass and shape of firebrands may not

realistic. Therefore, the models' validity can be improved by accounting for both mass and shape changes of firebrands with time during transport.

As some models generalizing firebrand transport only by plume effect is not adequate to neglect the effect of wind, turbulence and particle interactions and their influence on firebrand transport and deposition. Modelling fires with relevant HRR and permitting to create buoyancy by fire and surrounding flow interaction is encouraged in CFD models for firebrands lift and transport. The solution procedures used in each computational code can differ from one code to another creating deviations of results for a same fire event. We can assume institutional codes will specify and involve more physics to represent the coupled effects of fire and weather and their influence on other branches such as firebrands spotting and ignition. Conducting comprehensive validation processes is essential to increase the reliability of these CFD models. Investigating these aspects is still required in the computational modelling of firebrands to create a reliable integrated system to quantify the firebrand risk.

8. Operational model for spotting

There are multiple empirical, simulation and experimental studies available for the aspect of firebrand landing distribution, however, there is no comprehensive yet versatile approach for the application of these to operational fire spread models. There is a continuing demand for quick and efficient operational tools for firebrand management. Some of the operational platforms use Albini's empirical model (section 4.3) for spotting, for example, FARSITE [117] and BEHAVEPLUS [118]. From our previous discussion, we understand that Albini's model accounts for the maximum landing distance of firebrands, but it does not include any model for the spread of firebrands landing. Both these operational models use firebrand generation functions of Muraszew and Fedele [45].

FARSITE [117] uses a model based on Albini's [47] equations for spotting from torching trees. Torching trees produce many firebrands and are capable of lofting them high into the ambient winds. Therefore these are considered as a consistent source of firebrands. In FARSITE, instead of Eqs (13) and (14), firebrand's rate of travel in the horizontal direction (X) is determined by the windspeed at that height that decreases logarithmically toward the top of the canopy (h):

$$\frac{dX}{dt} = u_h \ln\left(\frac{z}{z_o}\right) \Big/ \ln\left(\frac{h}{z_o}\right) \tag{34}$$

where, z is the vertical position of firebrand calculated based on an equation similar to Eq (8), z_o is the friction length (0.4306 h) and u_h is the windspeed at height h

$$u_h = \frac{u_{h+20}}{\ln\left(\frac{20+1.18h}{0.43h}\right)} \tag{35}$$

Based on Eqs (34) and (35), the distance is calculated where the firebrand contacts with the ground surface.

BEHAVEPLUS [118] has burning pile and wind-driven surface fire models, besides a torching tree model. It may be noted that burning pile and torching tree models are for long range spotting, whereas the wind-driven surface fire model is designed to predict intermediate-range spotting. Short-range spotting such as debris blowing just across a fire line is not considered. The "maximum spotting distance" are calculated under "ideal" conditions Chase [64] models (Eqs (9)–(14)). BEHAV-EPLUS has four choices for spotting source, depending on the location of the fire in relation to the wind direction: ridgetop; midslope, leeward side; valley bottom; midslope, windward side (as shown in Fig. 14).

For the fast-moving eucalyptus forest fires, the Australian wildfire simulator, PHOENIX RapidFire [120], has included a module for firebrand transport where the quantity of firebrands generated is determined by the convective strength of the fire. It is assumed that due to the nature of Australian fuels, there is an order of magnitude more embers and some types can stay alight for long periods and traverse long distances compared to North American fuels (Ellis [23]). Therefore, PHOENIX uses a uniquely developed convection and surface wind model for firebrand transport, where fire-driven convection plays a key role in lofting embers. Short distance ember ignitions are included in PHOE-NIX's McArthur's forest model as an inherent part of the fire propagation mechanism (within 200 m of the firefront). The PHOENIX spotting model is designed for longer distance firebrands. Firebrands are transported at the speed and along the direction of the surface winds – this is a major limitation.

The firebrand generation from a burning cell is scaled between the arbitrary range of 0 and 60 embers/m^2 based on the cell's bark load (McCarthy et al. [121]).

$$available\ firebrand = \frac{1}{(1 + 108 \times \exp(-1.2 \times Bark\ load))} \quad (36)$$

The proportion of available firebrands launched and theoretical maximum ember 'hang-time'[8] in minutes are dependent on the convective strength at the cell's centre and are given by Eq (37) and (38).

$$firebrand\ porportion\ launched = 1.032$$
$$- \exp\left(4.5 \times 10^{-5} \times Convective\ Strength\right) \quad (37)$$

$$hang\ time = 0.6 \times Convective\ Strength\ /10000 \quad (38)$$

It is assumed that only a small proportion of all the firebrands launched, will reach the ground in a condition that could result in igniting a spot fire while the majority will be burned in air. An assumption is made that the total number of viable firebrands reaching the ground is inversely proportional to hang-time.

$$total\ viable\ firebrand = firebrand\ launched\ \times \exp\left(-9 \times \frac{hang\ time}{35}\right) \quad (39)$$

For each launch event, an empirically fitted 'resultant' spatial firebrand density distribution is used for each launch event and distributed across the landscape. According to Sardoy et al. [104] the best fit to observed spotting patterns can be provided by a Weibull/bimodal distribution. In a Weibull distribution based on hang time, for small convective values, the majority of firebrands are assumed to fall within a short time of launch at a short distance, however, as the hang-time increases, the majority of the firebrands land at a greater distance. Lateral firebrand distribution is also modelled using a Weibull function. Overall, the firebrand distribution is bimodal (wind dominated or plume dominated) along the travel path and perpendicular to the travel path firebrands are normally distributed with a standard deviation derived from the lateral spread Weibull function.

PHOENIX RapidFire also includes an ignition probability model

(based on FMC) for the spot fire spread. For this model, the fire spread due to spotfire was calibrated for eucalyptus forest which needs recalibration for other types of fuels [122]. The new operational platforms like WRF-SFIRE [123] and FOREFIRE [124] are fast and allow coupling between fires and atmosphere for better representation of atmospheric conditions, but they don't have any module for the spot-fire behaviour.

9. Future direction of research

By reviewing over a hundred articles, we can observe that firebrands generation, transportation, landing and the ignition of fuel beds or structures are the main aspects that have been studied in the past, mostly in isolation. Quantification of firebrand generation is one of the fundamental aspects which received little attention until recently. Hardly any studies have been conducted to directly measure firebrand generation (as a function of HRR or mass loss rate) from trees or forest burnings from the crown locations. Using infrared or other sophisticated cameras, followed by machine learning-based image post-processing firebrand generation rate could be measured.

The firebrand generation rate can vary due to numerous factors including vegetation type, fuel load, relative humidity (RH), air temperature, and driving wind velocities. Some studies were conducted to understand the variation of firebrand landing distribution (via collecting firebrands in collection trays away from the burning vegetation) as a function of these parameters. Attempts have also been made to interpolate firebrand landing data to obtain the firebrand generation rate at the source (crown locations). However, there is a need to integrate all these data to generate a simple model of firebrand generation rate as a function of HRR (includes both convective and radiative strength). Further adjustments can be made as a function of driving wind, fuel species and FMC (usually FMC captures the effect of RH and air temperature). This simple model could be used for providing input values for a physics-based model to model trajectories of firebrand transport from the source to the landing surface (ground, another tree or forest, or structure).

There is also a need to expand the experimental work on firebrand generation rate to include diverse vegetation types, including eucalypt species, to aid in benchmarking the transferability and applicability of data from around the world.

Physics-based models can simulate pyrolysis rates leading to combustion. A firebrand break-off model can also be included. However, for field-scale simulation using these options can be computationally enormously expensive. The option described in the immediately previous paragraph is a viable option with the current level of computational resources available. However, in the future, computational resources will increase, allowing the possibility of developing physics-based models which include firebrand generation rate as a function of dry mass loss rate. Both pyrolysis and firebrand generation are included in dry mass loss. Appropriate proportion needs to be provided from experimental studies.

For operational forecasting, which needs an ensemble of many parametric simulations, the use of physics-based modelling is still decades away. In Section 8, the current state of the firebrand submodel within operational models have been described. The submodels are very coarse approximations and primarily include landing distance of firebrands and some lateral dispersion. Experimentally validated physics-based models can be used to simulate a variety of wildfire conditions and develop a more refined, but computationally inexpensive model for landing contours to be used in operational models.

Investigating the effect of the sub-canopy wind and height from which firebrands are released could be a branch of future research to investigate the spotting distance and ignition potential. It is evident from various literature reviewed earlier that the sub-canopy wind has a major role in controlling the generation, transport and ignitability of these firebrands. During a fire spread, the burning of vegetation reduces the density of fuel and generates convective plumes; these result in changes

---

[8] represents the maximum time a firebrand ember can remain aloft.

in the sub-canopy wind.

Furthermore, the ignition process (and then sustaining and growing) of surface fuel or structures when interacting with a firebrand is complex as observed in the literature and other reviews. Most of the studies are carried out in a controlled laboratory environment using a regular-shape or idealised metallic firebrand particles. The interacting surface (where the heat transfer occurs) of firebrand and fuel is difficult to understand and significantly computationally expensive. Experimental studies should be conducted on ignition by firebrand to develop simple equations for operational models. The equations may be related to threshold conditions of fuel bed characteristics (bulk density, fuel bed packing factor, fuel load, fuel height, fuel moisture and thermal diffusivity) and atmospheric conditions (temperature, relative humidity and wind velocity) that coupled with spotting distribution model will assist in improving the accuracy of operational models.

10. Conclusion

A significant proportion of the risk posed to communities by wildfires is ultimately caused by firebrands. Spotting may substantially increase the rate of spread of wildfires given the right conditions, and a large proportion of wildfire-related property damage is caused by firebrand attacks. Modelling the transport and distribution (deposition) of firebrands is therefore an area of significant importance in research. The generation rate of firebrand is as an important aspect leading to transport and deposition but is often overlooked.

The present review focuses on understanding the current state of knowledge in generation and transport of firebrands and future direction it is taking forward. Understanding the transport of firebrands is a relatively new research area as compared to research carried out in understanding the fire spread modelling (with implicit effect of spotting). The knowledge in this domain has been notably boosted after the construction of artificial firebrand generators to carry out research in a controlled environment. Utilising this equipment has opened a new passage in understanding the dynamics behind the transport of firebrands and their landing distribution.

In this study, we reviewed both empirical and numerical studies which can assist in improvement of numerical models such as computational fluid dynamics (CFD) based modelling. In turn, CFD-based modelling will be able to assist in improving the performance of current operational models used by fire and emergency services through targeted parametric studies. In this review, particular emphasis is given on short-range firebrands due to their importance and difficulty to study other range firebrands due to resource-constraints. Studies involving ignition by firebrands have not been included in this study as it falls outside our focus areas. Based on our conducted review, we have presented a set of future research directions.

Funding

Declaration of Competing Interest

The authors declare that they have no known competing financial interests or personal relationships that could have appeared to influence the work reported in this paper.

Data availability

No data was used for the research described in the article.

References

[1] Y. Faxi, L. Rui, M. Ouejdane, An information system for real-time critical infrastructure damage assessment based on crowdsourcing method: a case study in Fort McMurray, in: International Conference on Sustainable Infrastructure 2017, 2017, pp. 96–103.

[2] R.N. McLeod, S.M. Pascoe, B.G. Teague, Final Report, Royal Commission into Victoria's Bushfires, The State of Victoria, Australia, 2010.

[3] C. Miller, et al., Electrically caused wildfires in Victoria, Australia are over-represented when fire danger is elevated, Landsc. Urban Plann. 167 (2017) 267–274.

[4] M. Ahrens, Brush, Grass, and Forest Fires, National Fire Protection Association, Fire Analysis and Research Division, 2013.

[5] V. Masson-Delmotte, et al., Climate Change 2021: the Physical Science Basis. Contribution of Working Group I to the Sixth Assessment Report of the Intergovernmental Panel on Climate Change, IPCC, Geneva, Switzerland, 2021.

[6] W.M. Jolly, et al., Climate-induced variations in global wildfire danger from 1979 to 2013, Nat. Commun. 6 (2015). Art. no. 7537.

[7] F. Tedim, et al., Defining extreme wildfire events: difficulties, challenges, and impacts, Fire 1 (1) (2018). Art. no. 9.

[8] J.J. Sharples, et al., Natural hazards in Australia: extreme bushfire, Climatic Change 139 (1) (2016) 85–99.

[9] A.L. Sullivan, Inside the inferno: fundamental processes of wildland fire behaviour. Part 1: combustion Chemistry and Heat Release, Curr. For. Rep. 3 (2) (2017) 132–149.

[10] A. Filkov, et al., Investigation of firebrand production during prescribed fires conducted in a pine forest, Proc. Combust. Inst. 36 (2) (2017) 3263–3270.

[11] A.C. Fernandez-Pello, Wildland fire spot ignition by sparks and firebrands, Fire Saf. J. 91 (2017) 2–10.

[12] N. Watson, G. Morgan, D. Rolland, The Bright Plantation Fire November, 1982, Division of Forest Protection, Forests Commission, Victoria, 1983.

[13] P. Billing, Some Aspects of the Behaviour of the Caroline Fire of February 1979, Division of Forest Protection, Forests Commission Victoria, 1980.

[14] R. Blanchi, J. Leonard, Investigation of Bushfire Attack Mechanisms Resulting in House Loss in the ACT Bushfire 2003, Bushfire CRC, 2005.

[15] A. Maranghides, W. Mell, A case study of a community affected by the Witch and Guejito wildland fires, Fire Technol. 47 (2) (2011) 379–420.

[16] S.L. Manzello, S. Suzuki, M.J. Gollner, A.C. Fernandez-Pello, Role of firebrand combustion in large outdoor fire spread, Progr. Energy Combust. Sci. Technol. 76 (2020), 100801.

[17] N. McCarthy, A. Guyot, A. Dowdy, H. McGowan, Wildfire and weather radar: a review, J. Geophys. Res. Atmos. 124 (1) (2019) 266–286.

[18] W. Węgrzyński, T. Lipecki, Wind and fire coupled modelling—part I: literature review, Fire Technol. 54 (5) (2018) 1405–1442.

[19] G.M. Byram, Combustion of Forest Fuels, Forest fire: control and use, 1959, pp. 61–89.

[20] A.G. McArthur, Fire Behaviour in Eucalypt Forests, Department of National Development, Commonwealth of Australia, Canberra, Australia, 1967.

[21] N. Cheney, G. Bary, The propagation of mass conflagrations in a standing eucalypt forest by the spotting process, in: Mass Fire Symposium, Defense Standards Laboratory, Melbourne, Australia, 1969, pp. 10–12.

[22] G.M. Byram, Atmospheric conditions related to blowup fires," Station Paper SE-SP-35. Asheville, NC: USDA-Forest Service, 36, Southeastern For. Exp. Stat. 35 (1954) 1–36.

[23] P.F. Ellis, The Aerodynamic and Combustion Characteristics of Eucalypt Bark: a Firebrand Study, PhD Dissertation, 2000. Australian National University.

[24] P.F. Ellis, The likelihood of ignition of dry-eucalypt forest litter by firebrands, Int. J. Wildland Fire 24 (2) (2015) 225–235.

[25] S.L. Manzello, T.G. Cleary, J.R. Shields, J.C. Yang, Ignition of mulch and grasses by firebrands in wildland–urban interface fires, Int. J. Wildland Fire 15 (3) (2006) 427–431.

[26] M.G. Cruz, J.S. Gould, M.E. Alexander, A.L. Sullivan, W.L. McCaw, S. Mathews, Guide to Rate of Fire Spread Models for Australian Vegetation, CSIRO Land and Water Flagship, 2015. Canberra, ACT and AFAC, Melbourne, VIC.

[27] J.S. Gould, W. McCaw, N. Cheney, P. Ellis, I. Knight, A. Sullivan, Project Vesta: Fire in Dry Eucalypt Forest: Fuel Structure, Fuel Dynamics and Fire Behaviour, CSIRO Publishing, Melbourne, Australia, 2008.

[28] M. Cruz, et al., Anatomy of a Catastrophic Wildfire: the Black Saturday Kilmore East Fire in Victoria, Australia, vol. 284, Forest Ecology and Management, 2012, pp. 269–285.

[29] P.A. Werth, et al., Synthesis of Knowledge of Extreme Fire Behavior: Volume I for Fire Managers, Joint Fire Science Program, 2011.

[30] I. Kaur, A. Mentrelli, F. Bosseur, J.-B. Filippi, G. Pagnini, Turbulence and fire-spotting effects into wild-land fire simulators, Commun. Nonlinear Sci. Numer. Simulat. 39 (2016) 300–320.

[31] R.H. Luke, A.G. McArthur, Bushfires in Australia, Australia Australian Government Publishing Service for CSIRO., Canberra, 1978.

[32] R. Rawson, P. Billing, S. Duncan, The 1982–83 forest fires in Victoria, Aust. For. 46 (3) (1983) 163–172.

[33] A.J. Buckley, Fire Behaviour and Fuel Reduction Burning, Bemm River Wildfire, October 1988, Fire Protection Branch, Department of Conservation & Environment, 1990.

[34] A. Bartlett, A Case Study of Wildfire Management in the Byadbo and Tingaringy Wilderness Areas, Fire Management Branch, 1993. Department of Conservation and Natural Resources.

[35] N. Cheney, Predicting forest fire behaviour–the Australian experience, in: Proceedings of the Workshop Integrating Research on Hazards in Fire-Prone Environments, The US Man and the Biosphere Program, 1991.

[36] F.A. Albini, Potential Spotting Distance from Wind-Driven Surface Fires, US Department of Agriculture, Forest Service, Intermountain Forest and Range Experiment Station, 1983.

[37] M. Raupach, Similarity analysis of the interaction of bushfire plumes with ambient winds, Math. Comput. Model. 13 (12) (1990) 113–121.

[38] N. Burrows, Describing Forest Fires in Western Australia: a Guide for Fire Managers, Forests Department, Perth, Western Australia, 1984.

[39] D.H. Ashton, Studies of litter in Eucalyptus regnans forests, Aust. J. Bot. 23 (3) (1975) 413–433.

[40] E.M. Birk, Overstorey and understorey litter fall in a eucalypt forest: spatial and temporal variability, Aust. J. Bot. 27 (2) (1979) 145–156.

[41] A.S. Macaulay, An Investigation of the Impacts of Massive Short Distance Spotting on the Forward Rate of Spread of Forest Fires, Master Research Dissertation, 2003. Institute of Land and Food Resources, University of Melbourne.

[42] M.G. Cruz, M.E. Alexander, Uncertainty associated with model predictions of surface and crown fire rates of spread, Environ. Model. Software 47 (2013) 16–28.

[43] A. Sullivan, Convective Froude number and Byram's energy criterion of Australian experimental grassland fires, Proc. Combust. Inst. 31 (2) (2007) 2557–2564.

[44] D. Morvan, G. Accary, S. Meradji, N. Frangieh, O. Bessonov, A 3D physical model to study the behavior of vegetation fires at laboratory scale, Fire Saf. J. 101 (2018) 39–52.

[45] A. Muraszew, J. Fedele, Statistical Model for Spot Fire Spread, The Aerospace Corporation Report No. ATR-77758801.(Los Angeles, CA), 1976.

[46] A. Muraszew, J. Fedele, W. Kuby, Investigation of Fire Whirls and Firebrands, Northern Forest Fire Laboratory, 1976. Intermountain Forest and Range Experiment Station.

[47] F.A. Albini, Spot Fire Distance from Burning Trees," Intermountain Forest and Range Experiment Station Missoula, MT, 1979. General Technical Report.

[48] M. El Houssami, et al., Experimental procedures characterising firebrand generation in wildland fires, Fire Technol. 52 (3) (2016) 731–751.

[49] S.L. Manzello, E.I. Foote, Characterizing firebrand exposure from wildland–urban interface (WUI) fires: results from the 2007 Angora Fire, Fire Technol. 50 (1) (2014) 105–124.

[50] S.L. Manzello, A. Maranghides, J.R. Shields, W.E. Mell, Y. Hayashi, D. Nii, Mass and size distribution of firebrands generated from burning Korean pine (Pinus koraiensis) trees, Fire Mater.: Int. J. 33 (1) (2009) 21–31.

[51] W. Mell, A. Maranghides, R. McDermott, S.L. Manzello, Numerical simulation and experiments of burning douglas fir trees, Combust. Flame 156 (10) (2009) 2023–2041.

[52] F. Hines, K. Tolhurst, A.A. Wilson, G.J. McCarthy, Overall Fuel Hazard Assessment Guide, Victorian Government, Department of Sustainability and Environment, Melbourne, 2010.

[53] K.G. Tolhurst, D.W. Flinn, R.H. Loyn, A.A.G. Wilson, I. Foletta, Ecological Effects of Fuel Reduction Burning in a Dry Sclerophyll Forest: a Summary of Principal Research Findings and Their Management Implications, Forest Research Centre, Department of Conservation and Environment, 1992.

[54] A. Hodgson, Control burning in eucalypt forests in Victoria, Australia, J. For. 66 (8) (1968) 601–605.

[55] W.L. McCaw, Behaviour and Short Term Effects of Two Fires in Regenerated Karri (Eucalyptus Diversicolor) Forest, 1986. *Technical Report-Western Australian Department of Conservation and Land Management (Australia)*.

[56] E. Koo, P.J. Pagni, D.R. Weise, J.P. Woycheese, Firebrands and spotting ignition in large-scale fires, Int. J. Wildland Fire 19 (7) (2010) 818–843.

[57] A.G. McArthur, Forest Fire Danger Meter, Forest Research Institute, Forestry & Timber Bureau, 1973.

[58] I. Noble, A. Gill, G. Bary, McArthur's fire-danger meters expressed as equations, Aust. J. Ecol. 5 (2) (1980) 201–203.

[59] C.S. Tarifa, Transport and Combustion of Firebrands, vol. 2, Instituto Nacional de Tecnica Aeroespacial, Esteban Terradas, Madrid, Spain, 1967.

[60] C.S. Tarifa, P.P. del Notario, F.G. Moreno, On the flight paths and lifetimes of burning particles of wood, in: Proceeding of Combustion Institute, vol. 10, 1965, pp. 1021–1037.

[61] A. Muraszew, W. Kuby, J. Fedele, Firebrand Investigation, Aerospace Corporation, 1975.

[62] F.A. Albini, Spot Fire Distance from Isolated Sources: Extensions of a Predictive Model, US Dept. of Agriculture, Forest Service, 1981. Intermountain Forest and Range Experiment Station.

[63] F. Albini, Transport of firebrands by line thermals, Combust. Sci. Technol. 32 (5–6) (1983) 277–288.

[64] C.H. Chase, *Spotting Distance from Wind-Driven Surface Fires: Extensions of Equations for Pocket Calculators* (No. 346), US Dept. of Agriculture, Forest Service, Intermountain Forest and Range Experiment Station, 1984.

[65] J.P. Woycheese, P.J. Pagni, D. Liepmann, *Brand Lofting above Large-Scale Fires*. Building and Fire Research Laboratory, National Institute of Standards and Technology, 1998.

[66] S.-L. Lee, J. Hellman, Study of firebrand trajectories in a turbulent swirling natural convection plume, Combust. Flame 13 (6) (1969) 645–655.

[67] H.R. Baum, B. McCaffrey, Fire induced flow field-theory and experiment, in: Proceedings of Fire Safety Science, vol. 2, 1989, pp. 129–148.

[68] J.P. Woycheese, P.J. Pagni, D. Liepmann, Brand propagation from large-scale fires, J. Fire Protect. Eng. 10 (2) (1999) 32–44.

[69] J. Woycheese, P. Pagni, Combustion models for wooden brands, in: Proceeding 3rd International Conference on Fire Research and Engineering, Society of Fire Protection Engineers, Washington, USA, 1999, p. 53.

[70] A. Tohidi, N.B. Kaye, Comprehensive wind tunnel experiments of lofting and downwind transport of non-combusting rod-like model firebrands during firebrand shower scenarios, Fire Saf. J. 90 (2017) 95–111.

[71] S.L. Manzello, J.R. Shields, J.C. Yang, Y. Hayashi, D. Nii, On the use of a firebrand generator to investigate the ignition of structures in wildland–urban interface (WUI) fires, in: Proceeding of 11th International Conference on Fire Science and Engineering, INTERFLAM, 2007, pp. 3–5.

[72] S.L. Manzello, T.G. Cleary, J.R. Shields, A. Maranghides, W. Mell, J.C. Yang, Experimental investigation of firebrands: generation and ignition of fuel beds, Fire Saf. J. 43 (3) (2008) 226–233.

[73] S.L. Manzello, A. Maranghides, W.E. Mell, Firebrand generation from burning vegetation, Int. J. Wildland Fire 16 (4) (2007) 458–462.

[74] T.R. Hudson, R.B. Bray, D.L. Blunck, W. Page, B. Butler, Effects of fuel morphology on ember generation characteristics at the tree scale, Int. J. Wildland Fire 29 (11) (2020) 1042–1051.

[75] S. Adusumilli, T. Hudson, N. Gardner, D.L. Blunck, Quantifying production of hot firebrands using a fire-resistant fabric, Int. J. Wildland Fire 30 (2) (2020) 154–159.

[76] B. Bahrani, Characterization of Firebrands Generated from Selected Vegetative Fuels in Wildland Fires, PhD Dissertation, 2020. The University of North Carolina at Charlotte.

[77] J. Song, X. Huang, N. Liu, H. Li, L. Zhang, The wind effect on the transport and burning of firebrands, Fire Technol. 53 (4) (2017) 1555–1568.

[78] D. Nguyen, N.B. Kaye, Quantification of ember accumulation on the rooftops of isolated buildings in an ember storm, Fire Saf. J. 128 (2022).

[79] D. Nguyen, N.B. Kaye, The role of surrounding buildings on the accumulation of embers on rooftops during an ember storm, Fire Saf. J. 131 (2022), 103624.

[80] S.L. Manzello, et al., On the development and characterization of a firebrand generator, Fire Saf. J. 43 (4) (2008) 258–268.

[81] S.L. Manzello, S. Suzuki, Experimentally simulating wind driven firebrand showers in Wildland-Urban Interface (WUI) fires: overview of the NIST firebrand generator (NIST dragon) technology, Procedia Eng. 62 (2013) 91–102.

[82] S.L. Manzello, S.H. Park, J.R. Shields, Y. Hayashi, S. Suzuki, Comparison testing protocol for firebrand penetration through building vents: summary of BRI/NIST full scale and NIST reduced scale results, Technical Note (NIST TN) 1659 (2010).

[83] S.L. Manzello, S. Suzuki, Exposing decking assemblies to continuous wind-driven firebrand showers, Fire Saf. Sci. 11 (2014) 1339–1352.

[84] S.L. Manzello, S. Suzuki, Experimental investigation of wood decking assemblies exposed to firebrand showers, Fire Saf. J. 92 (2017) 122–131.

[85] S.L. Manzello, S. Suzuki, Y. Hayashi, Enabling the study of structure vulnerabilities to ignition from wind driven firebrand showers: a summary of experimental results, Fire Saf. J. 54 (2012) 181–196.

[86] S. Suzuki, E. Johnsson, A. Maranghides, S.L. Manzello, Ignition of wood fencing assemblies exposed to continuous wind-driven firebrand showers, Fire Technol. 52 (4) (2016) 1051–1067.

[87] K. Zhou, S. Suzuki, S.L. Manzello, Experimental study of firebrand transport, Fire Technol. 51 (4) (2015) 785–799.

[88] R. Wadhwani, D. Sutherland, A. Ooi, K. Moinuddin, G. Thorpe, Verification of a Lagrangian particle model for short-range firebrand transport, Fire Saf. J. 91 (2017) 776–783.

[89] R. Wadhwani, D. Sutherland, A. Ooi, K. Moinuddin, Firebrand transport from a novel firebrand generator: numerical simulation of laboratory experiments, Int. J. Wildland Fire 31 (6) (2022) 634–648.

[90] J. Hashempour, Investigating Potential of Metal Mesh to Contain Wildfires, PhD Dissertation, 2016. University of Southern Queensland.

[91] J. Hashempour, A. Sharifian, Effective factors on the performance of woven wire screens against leaf firebrand attacks, J. Fire Sci. 35 (4) (2017) 303–316.

[92] A. Sharifian, J. Hashempour, Wind tunnel experiments on effects of woven wire screens and buffer zones in mitigating risks associated with firebrand showers, Aust. J. Mech. Eng. (2018) 1–13.

[93] J.C. Thomas, et al., Investigation of firebrand generation from an experimental fire: development of a reliable data collection methodology, Fire Saf. J. 91 (2017) 864–871.

[94] K. Himoto, T. Tanaka, Transport of disk-shaped firebrands in a turbulent boundary layer, Fire Saf. Sci. 8 (2005) 433–444.

[95] K. McGrattan, S. Hostikka, R. McDermott, J. Floyd, C. Weinschenk, K. Overholt, Fire dynamics simulator user's guide, NIST - Spec. Publ. 1019 (6) (2013) 1–339.

[96] Y.-D. Kim, Y.J. TC, S.J. Baek, C.H. Gee, A. Shuman, A numerical study on the roof ignition due to scattering firebrand attack by Wind, in: Proceedings of WEIIK Symposium, 2010, pp. 245–250.

[97] U.D.F. Manual, ANSYS FLUENT 12.0, Theory Guide, 2009.

[98] C. Thomas, J.J. Sharples, J. Evans, The terminal-velocity assumption in simulations of long-range ember transport, Math. Comput. Simulat. 175 (2020) 96–107.

[99] E. Koo, R.R. Linn, P.J. Pagni, C.B. Edminster, Modelling firebrand transport in wildfires using HIGRAD/FIRETEC, Int. J. Wildland Fire 21 (4) (2012) 396–417.

[100] R. Linn, J. Reisner, J.J. Colman, J. Winterkamp, Studying wildfire behavior using FIRETEC, Int. J. Wildland Fire 11 (4) (2002) 233–246.

[101] R. Wadhwani, D. Sutherland, K. Moinuddin, Simulated transport of short-range embers in an idealised bushfire, in: Proceeding 6th International Fire Behavior and Fuels Conference, 2019. Sydney, Australia.

[102] M.A. Storey, O.F. Price, R.A. Bradstock, J.J. Sharples, Analysis of variation in distance, number, and distribution of spotting in Southeast Australian wildfires, Fire 3 (2) (2020) 10.

[103] A. Wickramasinghe, N. Khan, K. Moinuddin, Determining firebrand generation rate using physics-based modelling from experimental studies through inverse analysis, Fire 5 (1) (2022) 6.

[104] N. Sardoy, J. Consalvi, A. Kaiss, A. Fernandez-Pello, B. Porterie, Numerical study of ground-level distribution of firebrands generated by line fires, Combust. Flame 154 (3) (2008) 478–488.

[105] N. Sardoy, J.-L. Consalvi, B. Porterie, A.C. Fernandez-Pello, Modeling transport and combustion of firebrands from burning trees, Combust. Flame 150 (3) (2007) 151–169.

[106] L.W. Menzemer, Numerical Simulations of Brand Transport in Large Outdoor Fires, MSc Ghent University Ghent, Belgium, 2021.

[107] R. Wadhwani, Physics-based Simulation of Short-Range Spotting in Wildfires, PhD Thesis, College of Engineering and Sciences, 2019. Victoria University, Melbourne.

[108] A. Haider, O. Levenspiel, Drag coefficient and terminal velocity of spherical and nonspherical particles, Powder Technol. 58 (1) (1989) 63–70.

[109] S.D. Tse, A.C. Fernandez-Pello, On the flight paths of metal particles and embers generated by power lines in high winds—a potential source of wildland fires, Fire Saf. J. 30 (4) (1998) 333–356.

[110] S. Kortas, P. Mindykowski, J.L. Consalvi, H. Mhiri, B. Porterie, Experimental validation of a numerical model for the transport of firebrands, Fire Saf. J. 44 (8) (2009) 1095–1102.

[111] A. Tohidi, N.B. Kaye, Stochastic modeling of firebrand shower scenarios, Fire Saf. J. 91 (2017) 91–102.

[112] W. Thurston, J.D. Kepert, K.J. Tory, R.J. Fawcett, The contribution of turbulent plume dynamics to long-range spotting, Int. J. Wildland Fire 26 (4) (2017) 317–330.

[113] S. Bhutia, M. Ann Jenkins, R. Sun, Comparison of firebrand propagation prediction by a plume model and a coupled–fire/atmosphere large–eddy simulator, J. Adv. Model. Earth Syst. 2 (1) (2010).

[114] J.C. Pereira, J. Pereira, A.L. Leite, D. Albuquerque, Calculation of spotting particles maximum distance in idealised forest fire scenarios, J. Combust. (2015) 2015.

[115] R.A. Anthenien, D.T. Stephen, A.C. Fernandez-Pello, On the trajectories of embers initially elevated or lofted by small scale ground fire plumes in high winds, Fire Saf. J. 41 (5) (2006) 349–363.

[116] K.E. Atkinson, An Introduction to Numerical Analysis, John Wiley & Sons, 2008.

[117] M.A. Finney, FARSITE: Fire Area Simulator-Model Development and Evaluation, 2004.

[118] P.L. Andrews, BEHAVE: Fire Behavior Prediction and Fuel Modeling System: BURN Subsystem, Part 2, General technical report INT, USA), 1989.

[119] P.L. Andrews, BEHAVE: Fire Behavior Prediction and Fuel Modeling System: BURN Subsystem, Part 1, US Department of Agriculture, Forest Service, Intermountain Research Station, 1986.

[120] K. Tolhurst, B. Shields, D. Chong, Phoenix: development and application of a bushfire risk management tool, Aust. J. Emerg. Manag. 23 (4) (2008) 47–54.

[121] G.J. McCarthy, K.G. Tolhurst, K. Chatto, Overall Fuel Hazard Guide, Fire Management, Department of Natural Resources & Environment, 1999.

[122] L. Pugnet, D. Chong, T. Duff, K. Tolhurst, Wildland–urban interface (WUI) fire modelling using PHOENIX Rapidfire: a case study in Cavaillon, France, in: Proceedings of the 20th International Congress on Modelling and Simulation, 2013, pp. 1–6. Adelaide, Australia.

[123] J. Mandel, J.D. Beezley, A.K. Kochanski, Coupled atmosphere-wildland fire modeling with WRF 3.3 and SFIRE 2011, Geosci. Model Dev. (GMD) 4 (3) (2011) 591–610.

[124] J.-B. Filippi, F. Morandini, J.H. Balbi, D.R. Hill, Discrete event front-tracking simulation of a physical fire-spread model, Simulation 86 (10) (2010) 629–646.